Study on unmyelinated fibers in the corpus callosum and stria terminalis.

DOCTORAL DISSERTATION

A thesis submitted in partial fulfillment

of the requirements for the degree of

Doctor of Philosophy

By:

Risa Yamano

Supervisor:

Dr. Nobuyuki Nukina

Co-supervisor:

Dr. Haruko Miyazaki

Graduate School of Brain Science

Doshisha University

March 2022

Kyoto, Japan

Table of Contents

List of Figures and Tables

Abstract

The distribution and role of unmyelinated fibers in the central nervous system (CNS) have not been explored. Fibers in the CNS can be roughly divided into myelinated and unmyelinated fibers according to the presence or absence of a myelin sheath in the mid-axonal regions. The naked area of axons, called the nodes of Ranvier, is located between adjacent myelin internodes. The axonal plasma membrane at the nodes of Ranvier contains a high concentration of voltage-gated sodium channels that generate action potentials and allow the saltatory conduction of impulses along the axons. Thus, myelination has evolved as a means of jumping conduction and increasing the speed of transmission in vertebrates. Our brains contain both unmyelinated fibers and myelinated fibers, which were acquired during the process of evolution. Therefore, it is necessary to figure out where the unmyelinated fibers exist and what advantages they have over the myelinated fibers.

Unmyelinated fibers in the CNS are known to exist in hippocampal mossy fibers and cerebellar parallel fibers. However, specific markers for unmyelinated axons have not been discovered. Previously, we found that the expression of the sodium channel β4 subunit (β4) is reduced in the early stage of Huntington disease transgenic mice. We also revealed that the striatal projection fibers were unmyelinated via Z-stack confocal immunofluorescence and immunoelectron microscopy (immuno-EM) analyses using the specific antibody against the sodium channel β4 subunit. The results showed a diffuse staining pattern. Nav1.2, one of the sodium channels α subunits, also exists diffusely in

the striatal projection fibers suggesting that Nav1.2 could be a marker of unmyelinated fibers.

In this study, I examined a diffuse staining pattern and a dotted staining pattern of unmyelinated fibers using an anti-Nav1.2 antibody in mouse brains. Especially, I focused on the corpus callosum (CC) and stria terminalis (ST), where axon bundles and long projections were found, and which were stained diffusely by the anti-Nav1.2 antibody. The immunohistochemistry and immuno-EM analysis supported the hypothesis that the diffuse localization of Nav1.2 could be a universal marker for unmyelinated fibers throughout the CNS.

To investigate the role of unmyelinated fibers in the brain network, their origins should be identified. Small neuronal cell bodies with a diameter of approximately 10 μm called granular cells are known for the origin of well-known unmyelinated fibers, such as hippocampal mossy fibers and cerebellar parallel fibers in the CNS. The neurons extending striatal projection fibers, including medium spiny neurons, also have a small diameter. The part of the CC fibers and the ST fibers are derived from the neurons in the cerebral cortex and amygdala, respectively. Therefore, I assumed that the unmyelinated axons in the CC and the ST are projected from the neurons with a diameter of approximately 10 μm in the cortex and amygdala. To identify the cell bodies of neurons with unmyelinated fibers, which are Nav1.2-positive in the CC and ST, I performed three experiments. First, I estimated the location of the cell bodies of neurons with unmyelinated fibers. Since the anti-Nav1.2 antibody does not stain the cell body, I followed the Nav1.2-positive fibers before the cell body in the CC and ST. The results suggested that some of the unmyelinated fibers in the CC originated from the primary visual cortex (V1), and those in the ST originated from the central amygdala nucleus.

Next, I injected Biotinylated dextran amine (BDA), an anterograde tracer, into the V1 in the CC. BDA from the neuronal cell bodies with the size of 10 μm at the V1 traveled down the CC axons and went toward the terminal processes. Finally, to examine which cell layers the projection fibers came from, I prepared a mouse expressing *Scnn1a*^{Cre}-tdTomato. This mouse fluorescently labels the thick granular cell layer at the cortical fourth layer (L4) and their projection fibers. Those fibers were partly stained with anti-Nav1.2 antibody diffusely. The results suggested that some of the unmyelinated fibers in the CC originated from V1L4.

Mutations of the *SCN2A* gene encoding Nav1.2 are associated with neurological disorders. However, how these pathologies are related to the distribution of Nav1.2 in unmyelinated axons has not been studied. The CC and ST have also been associated with a variety of neurological and psychiatric disorders. Therefore, it is important to investigate the localization and role of unmyelinated fibers in the CNS to understand the pathogenesis of brain diseases and develop treatments.

Acknowledgment

I would like to express my deepest appreciation to my advisors, Dr. Nobuyuki Nukina, Dr. Haruko Miyazaki and Dr. Tomoyuki Yamanaka for their invaluable support and for providing their insight and expertise which greatly improved this study. The authors thank Dr. Soichiro Kakuta, the Laboratory of Morphology and Image Analysis, Research Support Center, Juntendo University Graduate School of Medicine for technical assistance with electron microscopy. I would also like to give special thanks to my dissertation committee, Dr. Shigeo Takamori, Dr. Jun Motoyama and Dr. Yoshito Masamizu for their advice, encouragement and constructive criticism that motivated me to broaden my perspectives regarding my research.

This work would not have been possible without the financial support of the Ministry of Education, Culture, Sports, Science and Technology (MEXT) and Doshisha University.

I am also thankful to the lab members for encouraging and supporting me through this entire process. In particular, I thank Dr. Hongsun Park for editing the English of this manuscript. I thank my considerate colleagues for their kind cooperation. Finally, I wish to extend my sincere gratitude to my family and friends for their understanding, support and encouragement throughout my study.

Abbreviation list

CNS: Central nervous system

PNS: Peripheral nervous system

CC: Corpus callosum

ST: Stria terminalis

IHC: Immunohistochemistry

EM: Electron microscopy

Immuno-EM: Immunoelectron microscopy

V1: Primary visual cortex

CEA: Central amygdala

PAEZ: Pre-axonal exclusion zone

AIS: Axon initial segment

Nav: Voltage-gated sodium channels

KCNQ: Ligand- and voltage-gated potassium channels

Kv: voltage-gated potassium channels

Caspr: Contactin-associated protein

MBP: Myelin basic protein

JXP: Juxtaparanode

IF: Immunofluorescence

BDA: Biotinylated dextran amine

L4: Fourth layer

VMH: Ventromedial nucleus of the hypothalamus

BST: Bed nucleus stria terminalis

RFP: Red fluorescent protein

PBS: Phosphate buffered saline

PFA: Paraformaldehyde

DAB: Diaminobenzidine

WT: Wild type

TG: Transgenic

Chapter Ⅰ. The diffuse distribution of Nav1.2 on mid-axonal regions is a marker of unmyelinated fibers in the central nervous system

1. Introduction

1.1. Myelinated axons and unmyelinated axons.

Neurons are composed of the cell body, dendrites, pre-axonal exclusion zone (PAEZ), axon initial segment (AIS), mid-axon and distal axon terminal (Nirschl et al., 2017). The major difference between myelinated and unmyelinated fibers is the presence or absence of a myelin sheath, and the naked area between the myelin sheaths is called the nodes of Ranvier (Fig. 1a). Myelin sheaths are assembled as highly specialized lipid-rich membranes by both oligodendroglial cells in the central nervous system (CNS) and Schwann cells in the peripheral nervous system (PNS) (Hildebrand et al., 1993, Hildebrand et al., 1994). The evolution of early vertebrates included the insulation of axons with multilayered myelin sheaths for 'saltatory' impulse propagation, improving nerve conduction velocity. Myelin sheaths accelerate nerve conduction by from 20- to 100-fold compared to the unmyelinated axons of the same diameter by facilitating saltatory action potential propagation (Castelfranco and Hartline, 2016). The unmyelinated axons are thinner than myelinated axons. (Saliani et al., 2017).

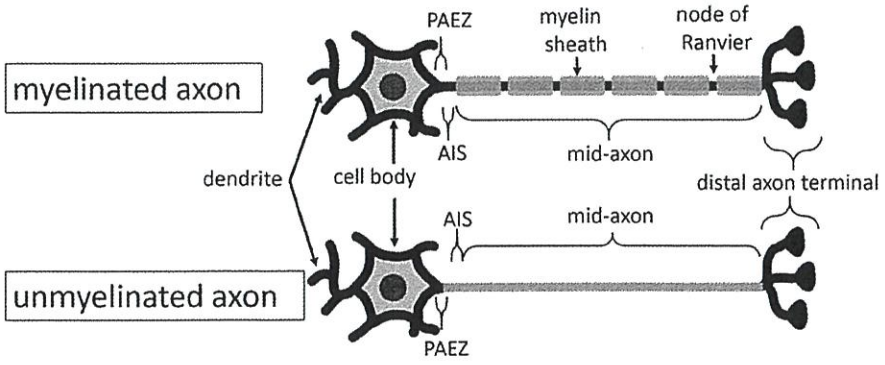

Figure 1. The difference between myelinated and unmyelinated axons.

(a) Schematic diagram of myelinated and unmyelinated fibers. PAEZ, pre-axonal exclusion zone; AIS, axon initial segment.

1.2. Markers of myelinated axons.

In myelinated axons, there are several kinds of channels and proteins: voltage-gated sodium channels (Nav), ligand- and voltage-gated potassium channels (KCNQ) and voltage-gated potassium channels (Kv) Kv3.1b channels at the nodes of Ranvier, Contactin-Associated Protein (Caspr) at paranodes, myelin basic protein (MBP) at myelin, and Kv1.1 and Kv1.2 channels at Juxtaparanode (JXP) under the compact myelin (Fig. 2) (Lai and Jan, 2006). In this study, Caspr and Nav were used as the markers of myelinated axons.

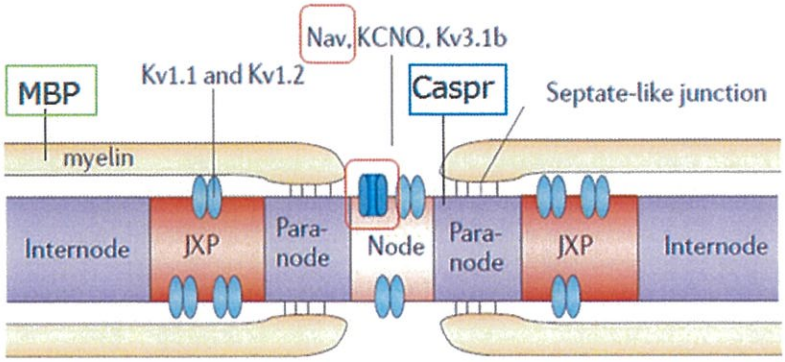

Figure 2. A typical channel and protein composition surrounding a myelinated axon.

The image was modified from (Lai and Jan, 2006).

1.3. Sodium channels.

Nav is a transmembrane glycoprotein complex that plays a critical role in the generation and propagation of action potentials in excitable cells, including neurons, and consists of one pore-forming α-subunit and one or two accessory β-subunits (Fig. 4). There are nine Nav α-subunit pore-forming isoforms encoded by different genes, Nav1.1 to Nav1.9, and an atypical non-voltage-dependent one, NavX (Table 1) (Catterall, 2012). In rodents, Nav1.3 is highly expressed in the fetal nervous tissues, whereas Nav1.1, Nav1.2 and Nav1.6 are abundant in the adult CNS. Nav1.2 encoded by *SCN2A* is expressed in excitatory neurons in the CNS and is important for neuronal excitability and synaptic depolarization, leading to neurotransmitter release (Li et al., 2014, Gong et al., 1999). Especially under physiological conditions, Nav1.2 permits the sodium influx from the extracellular space into the cytosol after depolarization of the nerve membrane. By postnatal day 30, Nav1.2 is progressively replaced by Nav1.6 in myelinated neurons and at the nodes of Ranvier, in particular (Boiko et al., 2001). Generally, Nav1.1 and Nav1.3 localize to the soma of neurons where they may control neuronal excitability through the integration of synaptic impulses in order to set the threshold for action potential initiation and propagation to the axonal compartments. Nav1.1 and Nav1.6 are also significantly expressed in the PNS. Nav1.7, Nav1.8 and Nav1.9 are the most abundantly expressed

sodium channel isoforms in the PNS that have been cloned from sympathetic and dorsal root ganglion neurons. Among these isoforms, Nav1.7 is the most broadly expressed in the PNS and appears to localize to axons where it may function in initiating and conducting the action potential (Toledo-Aral et al., 1997). More restricted expression patterns are observed for Nav1.8 and Nav1.9. These channels are differentially expressed in small sensory neurons of the dorsal root and trigeminal ganglia where they play a key role in the perception of pain (Black et al., 1999, Akopian et al., 1999). Finally, Nav1.4 and Nav1.5 are muscle sodium channels that control the excitability of the skeletal and cardiac myocytes, respectively (Goldin, 2001).

Five β-subunits have been identified in mammals: β1, the alternative splice variant β1B (previously called β1A), β2, β3 and β4. Each β-subunit is encoded by one of the four genes: *SCN1B*, *SCN2B*, *SCN3B* and *SCN4B*. β-subunits are highly expressed in excitable cells, including central and peripheral neurons and skeletal and cardiac muscle cells. They are also expressed in non-excitable cells such as astrocytes, radial glia and Bergmann glia (Table 1) (Baroni and Moran, 2015). Especially for the aforementioned β4 subunit encoded by *SCN4B*, the area expressing the gene is restricted to discreet brain regions, particularly to the dorsal striatum and the nucleus accumbens (Oyama et al., 2006, Miyazaki et al., 2014). The β4 subunit is known for mediating drugs of abuse's rewarding

properties (Feltenstein and See, 2008) and for preventing normal inactivation, conferring channels the ability to evoke a resurgent current upon repolarization (Bant and Raman, 2010).

Table 1. Types of human sodium channels α- and β-subunits and their tissue distribution.

The table was modified from (Baroni and Moran, 2015).

Gene	Chromosome	Protein	Uniprot code*	Tissue expression
α-subunits				
SCN1A	2q24.3	Nav1.1 or α1.1	P35498	Cell bodies of central neurons, T-tubules in myocytes axon initial segments
SCN2A	2q24.3	Nav1.2 or α1.2	Q99250	Central neurons, mainly localizated in unmyelinated and premyelinated axons
SCN3A	2q24.3	Nav1.3 or α1.3	Q9NY46	Cell bodies of central neurons, cardiac myocytes
SCN4A	17q23.3	Nav1.4 or α1.4	P35499	Skeletal muscles
SCN5A	3p21-22	Nav1.5 or α1.5	Q86V90	Cardiac myocytes, immature and denervated skeletal muscles, certain brain neurons
SCN8A	12q13	Nav1.6 or α1.6	Q9UQD0	Somatodendritic distribution in output neurons of cerebellum, cerebral cortex, hippocampus; Purkinje cells in cerebellar granule cell layer, astrocytes, Schwann cells, axon initial segments, dorsal root ganglia, nodes of Ranvier in peripheral and central nervous systems, T-tubules in cardiac myocytes
SCN9A	2q24	Nav1.7 or α1.6	Q15858	Dorsal root ganglia neurons, sympathetic neurons, Schwann cells, neuroendocrine cells
SCN10A	3p22.2	Nav1.8 or α1.8	Q9Y5Y9	Dorsal root ganglia neurons, human heart, intracardiac neurons
SCN11A	3p22.2	Nav1.9 or α1.9	Q9UI33	C-type neurons in dorsal root ganglia
SCN7A	2q24.3	NavX	Q01118	Dorsal root ganglia neurons, hippocampus, thalamus, cerebellum, median preoptic nucleus, circumventricular organs, Peripheral nervous system (PNS),
β-subunits				
SCN1B	19q13.1	SCN1b or β1	Q07699	Ubiquitous: central and peripheral neurons, glia, skeletal and cardiac muscles
SCN1B	19q13.1	SCN1bB or β1B		Cortical neurons, Cerebellar Purkinje cells, Deep cerebellar nuclei, Ventral horn neurons, Dorsal root ganglia neurons, peripheral nerves
SCN2B	11q23	SCN2b or β2	Q5U0K8	Central and peripheral neurons, glia, cardiac muscles
SCN3B	11q23.3	SCN3Bor β3	Q9NY72	Central and peripheral neurons, adrenal glands, kidney
SCN4B	11q23.3	SCN4b or β4	Q8IWT1	Central and peripheral neurons, glia, skeletal and cardiac muscles

1.4. Markers of unmyelinated axons.

1.4.1. β4 cannot be a specific marker for unmyelinated axons.

While many specific molecular markers for myelinated axons have been established with distinct localizations at the paranode and the nodes of Ranvier (Lai and Jan, 2006), specific markers for unmyelinated axons have not been discovered. Previously, Oyama *et al.* investigated the localization of the Nav β4 subunit in Huntington disease (HD) transgenic mice R6/2, which contains N-terminally truncated mutant huntingtin with the expansion of CAG repeat (~125 repeats) within the exon 1 of the *huntingtin* gene (Mangiarini et al., 1996), and found that the expression of the Nav β4 subunit is reduced in the early stage of the disease (Oyama et al., 2006). The β4 mRNA was expressed at the highest level in the striatum and the moderate level in the cerebral cortex layers III and V. In R6/2, by contrast, the expression of β4 was markedly reduced at the age of 8 weeks, especially in the striatum (Fig. 3a, b) (Oyama et al., 2006). β4 was distributed diffusely in the axons of the striatal projection neurons in the basal ganglia (Fig. 3c), which is different from the dotted distribution observed in the white matter of the cerebellum (Fig. 3d). For direct evidence that β4-expressing striatal projection axons are unmyelinated, immuno-EM analysis was performed with an antibody specific to the mouse β4 C-terminal peptide (anti-mSCN4B-C), which labels the unmyelinated axons in the fascicles

of striatal projection fibers in the striatum (Fig. 3e) (Miyazaki et al., 2014). Many unmyelinated fibers and myelinated fibers were found to be wrapped in myelin sheaths, and a mitochondrion was observed in the axons. Taken together, these results suggest that β4-expressing striatal projection axons are unmyelinated, raising the possibility that β4 could be a specific marker for unmyelinated axons. However, this diffuse staining pattern of the β4 subunits was found mainly in the striatal projection fibers. Therefore, the diffuse presence of the β4 subunits in the axons would not be a good marker of unmyelinated fibers in general.

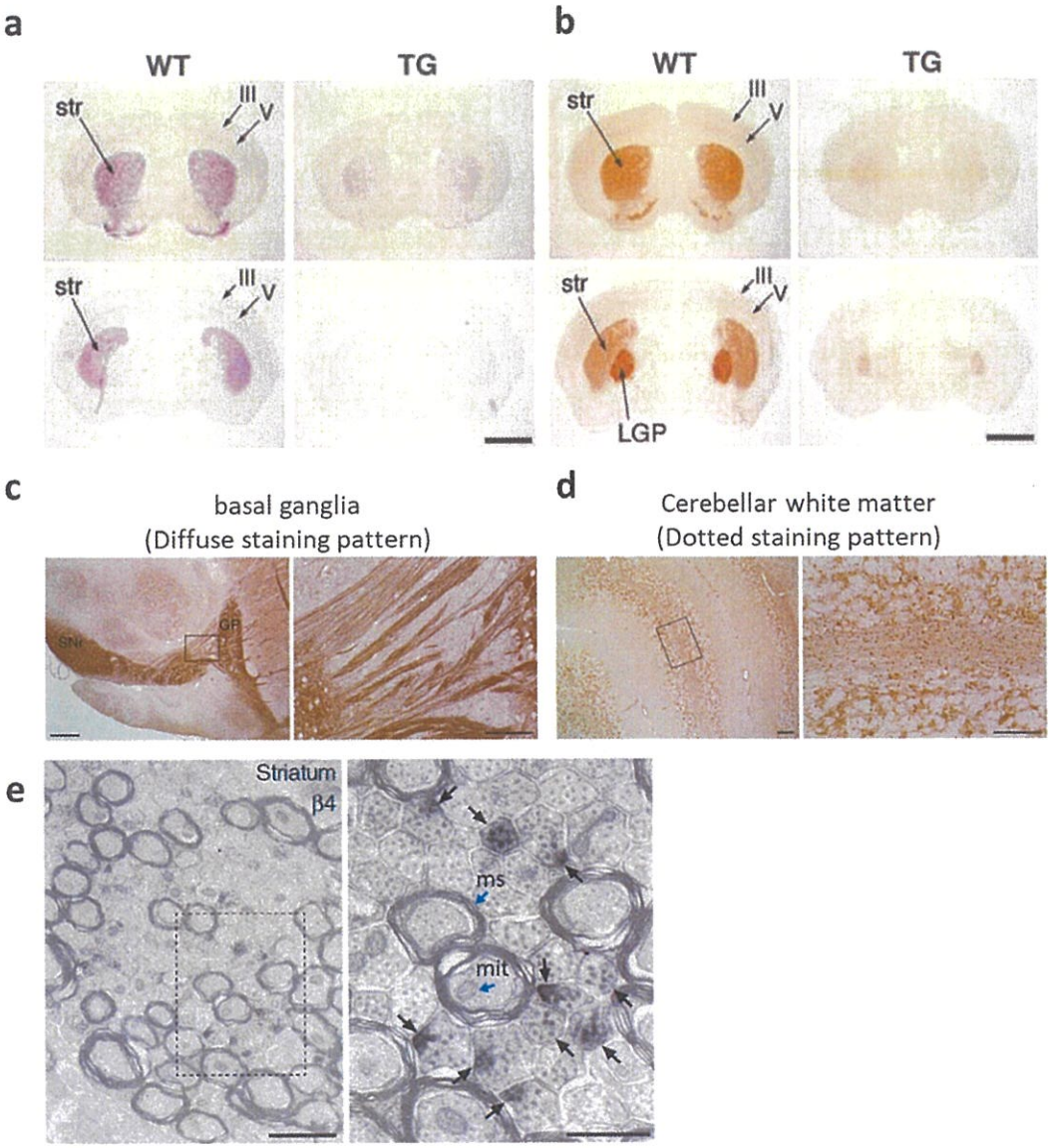
a
WT
TG
str
III
V
b
WT
TG
str
III
V
LGP
c
basal ganglia
(Diffuse staining pattern)
SNr
GP
d
Cerebellar white matter
(Dotted staining pattern)
e
Striatum
β4
ms
mit

Figure 3. The β4-expressing striatal projection axons are unmyelinated.

(a, b) The comparative distribution of the β4 subunit in the 8-week-old brain between wild type (WT) and R6/2 (TG) mice was investigated by *in situ* hybridization (a) and immunohistochemistry (b). (c, d) β4 expression in the 16-week-old mouse brain. The basal ganglia (c) and cerebellar white matter (d) were stained with the anti-mSCN4B-C antibody. The right panels show higher magnification of the boxed area in the left panels. (e) Immuno-EM analysis using the anti-mSCN4B-C antibody in striatal projection fibers. The right panel shows a higher magnification of the boxed area in the left panel. Arrows indicate the β4-labeled axons. The images were modified from (Oyama et al., 2006) (a, b) and (Miyazaki et al., 2014) (c-e). III and V, cerebral cortex layers III and V; str, striatum; Ot, olfactory tubercle; LGP, lateral globus pallidus; GP, globus pallidus; SNr, substantia nigra pars reticulata; ms, myelin sheet; mit, mitochondrion. Scale bars: 2 mm (a, b), 100 μm (c, left; d, right), 50 μm (c, right), 500 μm (d, left), 1 μm (e, left) and 0.5 μm (e, right).

1.4.2. Nav1.2 can be a marker of unmyelinated fibers.

The previous investigation has demonstrated that the Nav α-subunit or Nav1.2 could be a suitable marker for unmyelinated axons(Miyazaki et al., 2014). Nav consists of one pore-forming α-subunit and one or two accessory β-subunits (Fig. 4a). Since immunofluorescence (IF) staining revealed that the anti-Nav1.2 antibody-positive signals were diffusely distributed in the striatal axons, and their immunoreactivity co-localized with the anti-β4 antibody-positive signals (Fig. 4b), the α-subunit co-expressed with β4 in the striatal projection fibers might be Nav1.2. To confirm whether Nav1.2-expressing fibers are unmyelinated, IF staining was performed with the anti-Nav1.2 and anti-Caspr antibodies. The anti-Nav1.2 antibody-positive signals did not co-localize with the anti-Caspr antibody-positive signals (Fig. 4c). These results suggest that Nav1.2 is a major α-subunit of unmyelinated striatal projection fibers (Miyazaki et al., 2014). This specific localization of Nav1.2 was also reported by other studies (Ogiwara et al., 2018, Yamagata et al., 2017). The anti-β4 antibody was not appropriate to search for unmyelinated fibers in the mouse brain because the area stained by the antibody was limited to the striatal projection fibers. On the other hand, the anti-Nav1.2 antibody diffusely stained a wider area compared to the anti-β4 antibody. Therefore, I hypothesized that Nav1.2 could be a superior molecular maker to β4 of unmyelinated axons throughout the brain.

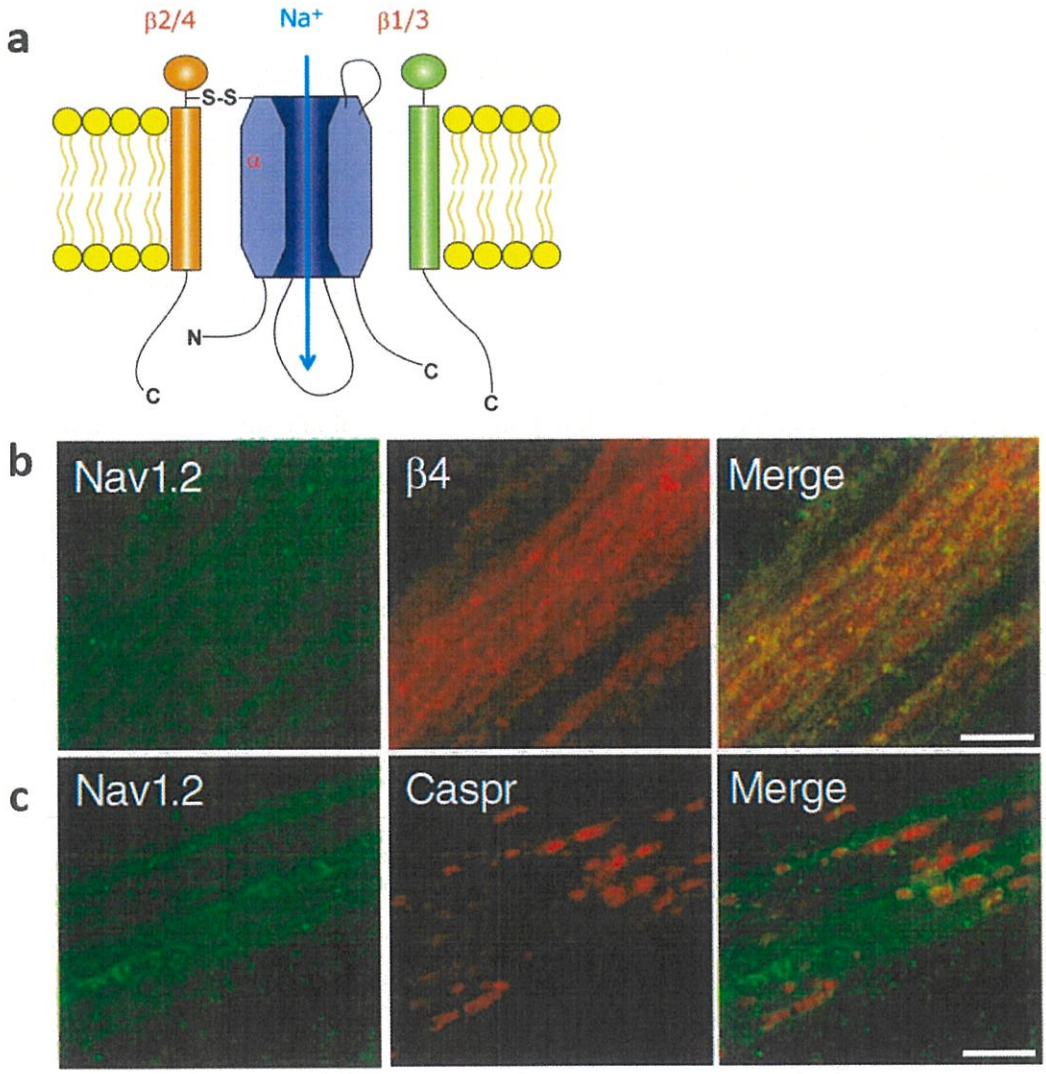

Figure 4. Nav1.2 is a major α-subunit of unmyelinated striatal projection fibers.

(a) a schematic diagram of a sodium channel. Courtesy of Dr. Haruko Miyazaki. (b, c) The sagittal sections of the striatal fascicles in the 17-week-old mice were stained with the anti-Nav1.2 (green) and anti-β4 (red) antibodies (b) and the anti-Nav1.2 (green) and anti-Caspr (red) antibodies (c). Scale bars: 5 μm. The images were modified from (Miyazaki et al., 2014) (b, c).

1.5. The aim of this chapter.

The distribution and the origin of unmyelinated fibers in the CNS have not been well determined because the characteristic markers of unmyelinated fibers remain unknown. Our brains contain both unmyelinated fibers and myelinated fibers, which were acquired during the process of evolution. However, the distribution and role of unmyelinated fibers in the CNS have not been explored. It is necessary to figure out where the unmyelinated fibers exist and what advantages they have over the myelinated fibers.

2. Results

2.1. Nav1.2 is a marker for unmyelinated fibers in the striatum.

Since Nav1.2 and Neurofilament-H (NFH) are distributed diffusely in the striatal axon bundles separately (Miyazaki et al., 2014), I hypothesized that NFH is distributed diffusely in myelinated axons, and the myelinated and unmyelinated fibers could be distinguished by their staining patterns. To identify the location of the Nav1.2-positive fibers in the striatum, mouse brain sections were stained with an antibody specific to Nav1.2. Multiple axon bundles were detected in the middle and the bottom of the striatum (Fig. 5a). Next, by using the antibodies specific to Nav1.2 and NFH (Fig. 5b), I performed double staining in the striatal axon bundles. In the coronal striatal sections, the axon bundles cut into rings were observed to identify proteins that were specifically expressed in the axons. The NFH-positive and the Nav1.2-positive axons did not overlap, forming their own bundles (Fig. 5c, upper panels). On the other hand, in the sagittal striatal sections, the axon bundles sectioned along with the fibers were observed to investigate the location of the proteins. Both Nav1.2 and NFH showed a diffuse staining pattern on the axon bundles, and their signals did not overlap (Fig. 5c, lower panels). These results suggest that the axons could be distinguished by these two types of antibodies. Since

myelinated fibers are characterized by the presence of the nodes of Ranvier, I next examined their presence or absence on the Nav1.2-positive and NFH-positive axons by IF staining on the sagittal striatal sections. The anti-Nav1.6 and anti-Caspr antibodies were used for triple staining with the anti-Nav1.2 or anti-NFH antibodies. If the nodes of Ranvier were present on the axons, a set of 'Caspr-Nav1.6-Caspr' staining might be observed on the axons. As almost no Caspr-Nav1.6-Caspr staining was observed on the Nav1.2-positive axons, these axons might be unmyelinated (Fig. 5d). On the contrary, the NFH-positive axons might be myelinated since Caspr immunoreactivities seemed to localize along the NFH-positive axons (Fig. 5e).

a

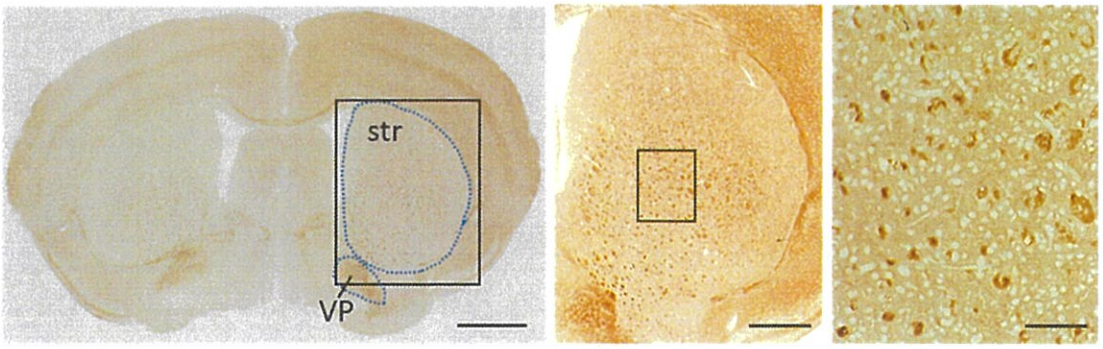

b

	Markers	Distribution
myelinated axons	NFH	cytoskeletal component
	Caspr	paranodes
	Nav1.6	node of Ranvier
unmyelinated axons	Nav1.2	

c

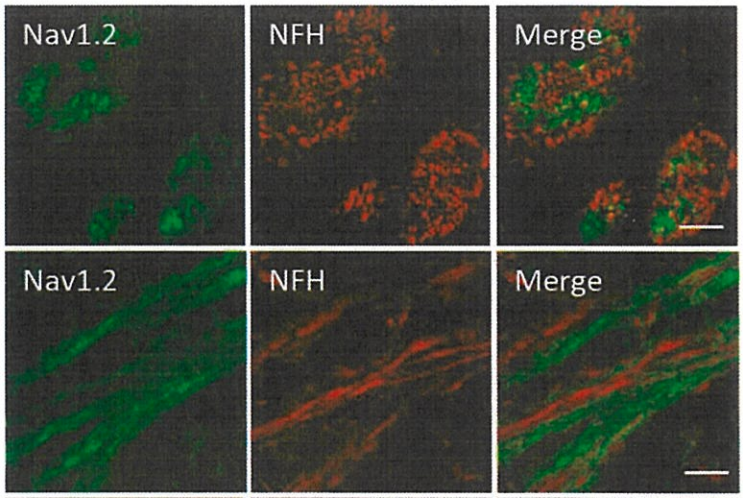

d

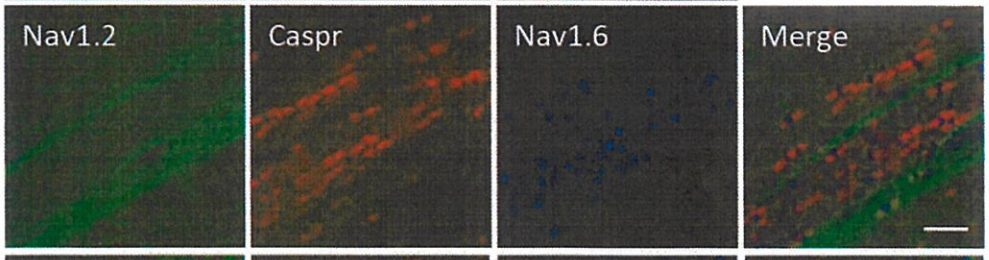

e

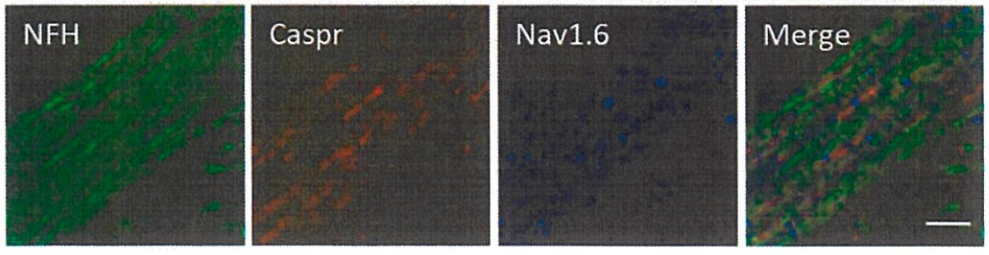

Figure 5. Characterization of the Nav1.2-expressing axons in the striatum.

(a, c) The mouse brain sections were stained with the (a) anti-Nav1.2, (c) anti-Nav1.2 (green) and the anti-NFH (red) antibodies. (a) The middle panel shows a higher magnification of the boxed area in the left panel, and the right panel shows a higher magnification of the boxed area in the middle panel. (b) A table of markers and their distribution. (d, e) The sagittal sections of the striatal fascicles in the 8-week-old mice were stained with the (d) anti-Nav1.2 (green), anti-Caspr (red) and anti-Nav1.6 (blue) antibodies, and the (e) anti-NFH (green), anti-Caspr (red) and anti-Nav1.6 (blue) antibodies. Scale bars: 1 mm (a, left), 500 μm (a, middle), 100 μm (a, right), 20 μm (c, d). str, striatum; VP, ventral pallidum.

To further confirm whether the myelinated and unmyelinated fibers could be distinguished by their staining patterns, I performed electron microscopy (EM) and immuno-EM analyses. The EM analysis showed that the fascicles of the striatal projection fibers were composed of a large number of unmyelinated axons (Fig. 6a). For immuno-EM analysis, the specimens were frozen and thawed, thereby breaking the cell membranes, to penetrate the antibodies. The anti-Nav1.2 antibody stained the surface and the interior part of unmyelinated fibers (Fig. 6b, left). On the contrary, myelinated axons

were labeled with the anti-NFH antibody (Fig. 6b, right). Taken together, I demonstrated that the Nav1.2-expressing axons were unmyelinated in the striatum. These results support the hypothesis that the diffuse localization of Nav1.2 could be a universal marker for unmyelinated fibers throughout the CNS.

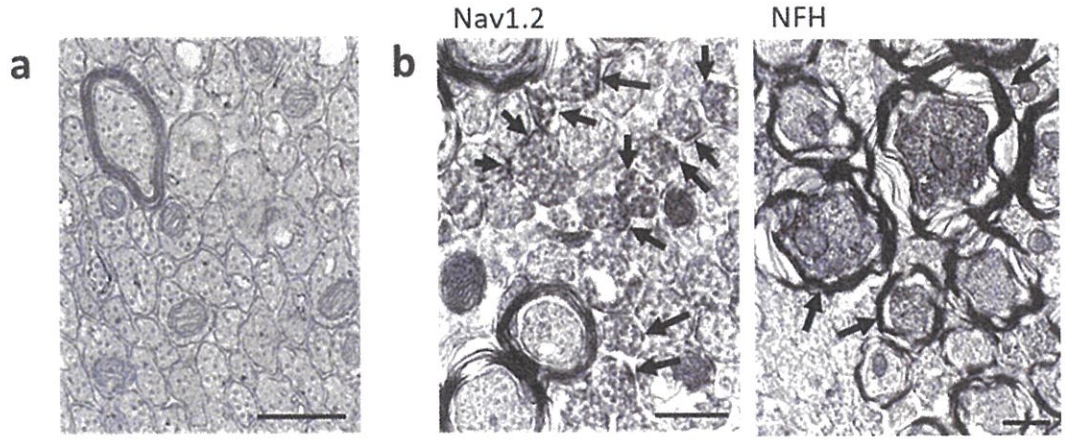

Figure 6. Unmyelinated axons in the striatum were stained with the anti-Nav1.2 antibody.

(a) The EM analysis of the cross-sectioned striatal projection fibers in the striatum. (b) The immuno-EM analysis using the anti-Nav1.2 (left) or anti-NFH (right) antibodies in the striatal projection fibers. Arrows indicate the Nav1.2- (left) or NFH- (right) labeled axons. Scale bars: 0.5 μm.

2.2. A unique distribution of Nav1.2 in the mouse brain.

To investigate the distribution of Nav1.2 in the CNS, immunohistochemistry (IHC) was performed on the sagittal mouse brain sections with the anti-Nav1.2 antibody (Fig. 7a). Several regions, including the well-known unmyelinated fibers in the CNS, such as hippocampal mossy fibers, cerebellar parallel fibers and striatal projection fibers, showed robust and fibrous labeling (Fig. 7b). In the same way, I examined whether there were any other regions with fibers stained with the anti-Nav1.2 antibody. As strong signals were detected in the corpus callosum (CC) and stria terminalis (ST) (Fig. 7c), which are known to contain axon bundles and long projections (Ku and Torii, 2020, Dong et al., 2001), I next investigated whether the antibody-positive fibers in these regions are unmyelinated.

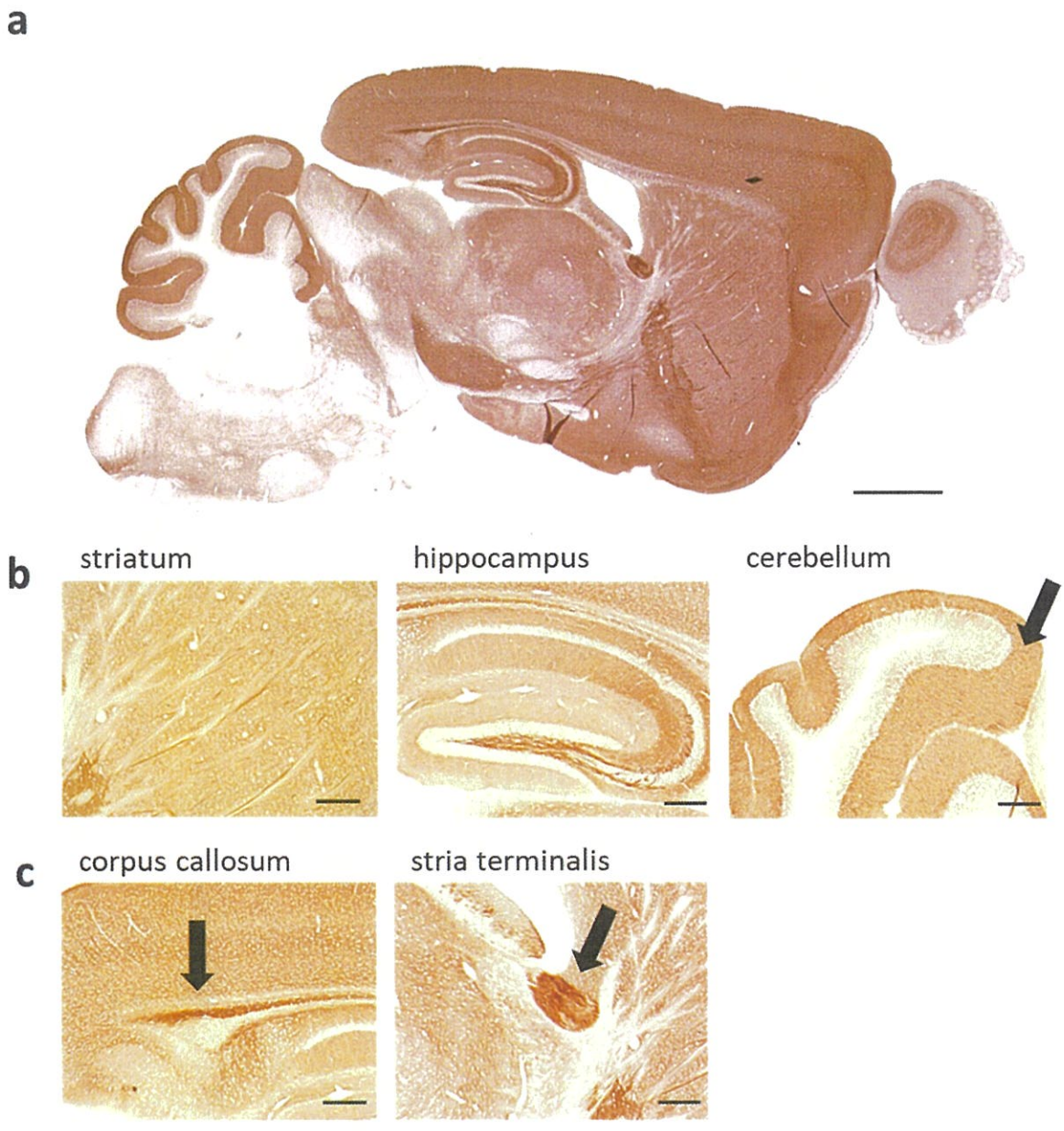
a
b
striatum
hippocampus
cerebellum
c
corpus callosum
stria terminalis

Figure 7. The distribution of Nav1.2 in the mouse brain.

(a) The expression of Nav1.2 in the mouse brain. (b, c) The expression of Nav1.2 in the striatum, hippocampus and cerebellum (b), and forceps major of corpus callosum and stria terminalis (c). Arrows indicate the Nav1.2-labeled axons. Scale bars: 1 mm (a), 200 μm (b, c).

2.3. Nav1.2 was found diffusely in the axons of neurons in the corpus callosum.

I paid special attention to the posterior part of the CC, which was more intensively stained than other parts of the CC, with the anti-Nav1.2 antibody. Double staining of the anti-Nav1.2 and anti-NFH antibodies was performed to distinguish axons at the microscopic level in the CC. Then, I examined the presence or absence of the nodes of Ranvier in the Nav1.2-positive axons by IF staining. The anti-Nav1.6 and anti-Caspr antibodies were used for triple staining with the anti-Nav1.2 or anti-NFH antibodies. The axons were supposed to be stained with the anti-Nav1.2 antibody in the coronal sections, suggesting the presence of unmyelinated fibers (Fig. 8a). I also confirmed that the anti-Nav1.2 antibody-positive and anti-NFH antibody-positive signals did not overlap. The Nav1.2-positive axons and the NFH-positive axons were detected in the CC and the

cingulate gyrus, respectively. In the coronal sections, the Nav1.2-positive axons were sectioned along with the fibers. The top of the axon bundles in the CC was Nav1.2-positive and NFH-negative, suggesting that they were unmyelinated (Fig. 8b). The nodes of Ranvier were not identified on the Nav1.2-positive axons, further supporting the result that the Nav1.2-positive axons were unmyelinated (Fig. 8c). At the NFH-positive axons above the CC, the signals detecting the nodes of Ranvier were not observed because the NFH-positive fibers above the CC are the axonal cross-sections that could not show the nodes of Ranvier on the axons (Fig. 8d).

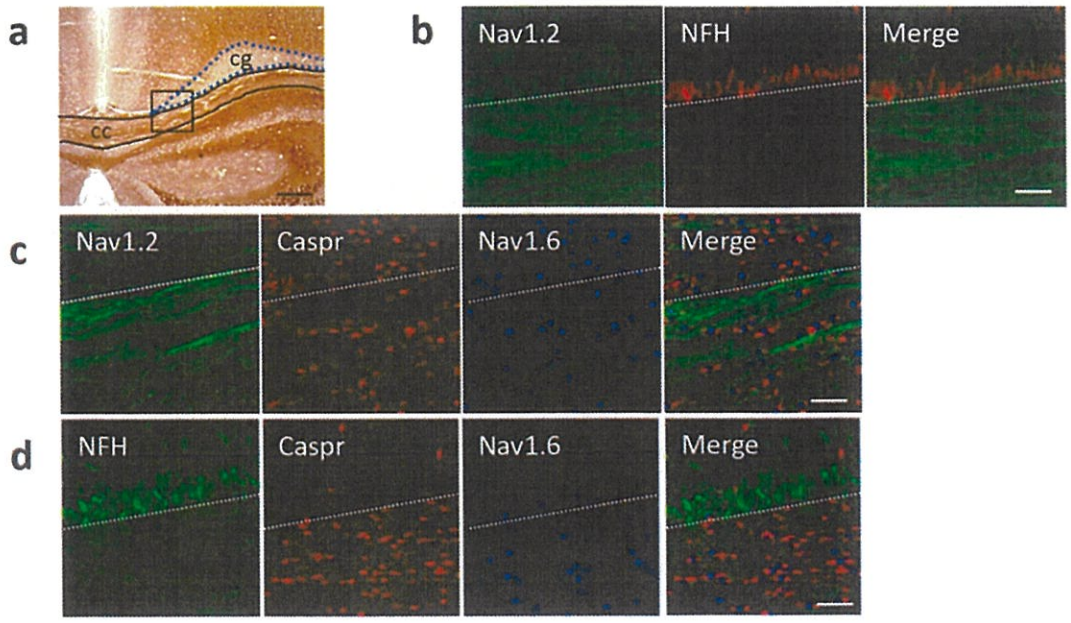

Figure 8. Characterization of the Nav1.2-expressing axons in the coronal sections of the corpus callosum.

(a-d) The coronal CC sections at 2 mm caudal to the bregma of the 8-week-old mice were stained with the (a) anti-Nav1.2, (b) anti-Nav1.2 (green) and anti-NFH (red), (c) anti-Nav1.2 (green), anti-Caspr (red) and anti-Nav1.6 (blue), and (d) anti-NFH (green), anti-Caspr (red) and anti-Nav1.6 (blue) antibodies. (a) The region circled in blue refers to the cingulate gyrus (cg). The region between the two black lines indicates the CC. (b-d) The panels show a higher magnification of the boxed area in (a). (a-d) The areas below the dotted lines show the CC. Scale bars: 100 μm (a), 20 μm (b-d).

In the sagittal sections cut at 0.48 mm lateral from the midline, the fibers were strongly stained with the anti-Nav1.2 antibody (Fig. 9a). As the previous result using the coronal sections, the anti-Nav1.2 antibody-positive and the anti-NFH antibody-positive signals did not overlap, and the Nav1.2-positive and the NFH-positive axons were observed in the CC and the cingulate gyrus, respectively. Because the Nav1.2-positive axons were cut on the cross-sections (Fig. 9b), it was difficult to determine whether the

nodes of Ranvier were present on the Nav1.2-positive axons (Fig. 9c). On the NFH-positive axons, the nodes of Ranvier were identified (Fig. 9d).

The EM and immuno-EM analyses showed that the fascicles of axons in the CC were composed of many unmyelinated axons (Fig. 10a). The surface and the interior part of unmyelinated axons were labeled by the anti-Nav1.2 antibody (Fig. 10b, left), and the internal part covered by the myelin sheaths was labeled by the anti-NFH antibody (Fig. 10b, right). Taken together, I demonstrated that the Nav1.2-positive unmyelinated axons exist in the CC.

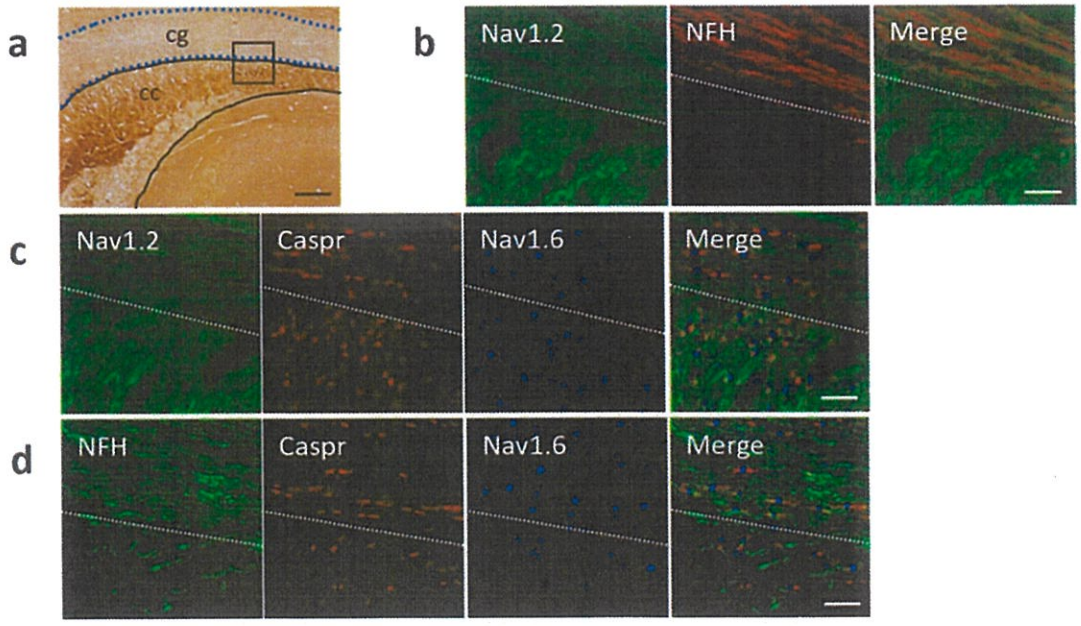

Figure 9. Characterization of the Nav1.2-expressing axons in the sagittal sections of the corpus callosum.

(a-d) The sagittal CC sections of the 8-week-old mice were stained with the (a) anti-Nav1.2, (b) anti-Nav1.2 (green) and anti-NFH (red), (c) anti-Nav1.2 (green), anti-Caspr (red) and anti-Nav1.6 (blue), and (d) anti-NFH (green), anti-Caspr (red) and anti-Nav1.6 (blue) antibodies. (a) The region between the two blue dotted lines refers to the cingulate gyrus (cg). The region between the two black lines indicates the CC. (b-d) The panels show a higher magnification of the boxed area in (a). (a-d) The areas below the dotted lines show the CC. Scale bars: 100 μm (a), 20 μm (b-d).

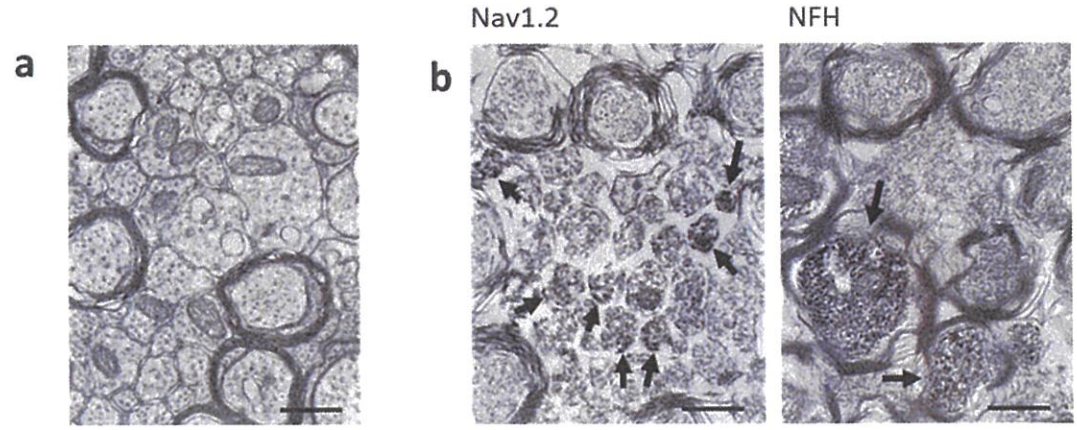

Figure 10. The Nav1.2-positive unmyelinated axons in the corpus callosum.

(a) The EM analysis in the sagittal CC sections. (b) The immuno-EM analysis using the anti-Nav1.2 (left) and anti-NFH (right) antibodies. Arrows indicate the Nav1.2- (left) or NFH- (right) labeled axons. Scale bars: 0.5 μm.

2.4. The Nav1.2-expressing axons in the stria terminalis are unmyelinated.

Next, using the same methods, I examined whether the Nav1.2-positive axons were present in the ST and whether they were unmyelinated. The axons in the ST form arc-shaped fiber bundles, which come from the amygdala and go back to the bed nucleus of the ST (BST) (Fig. 11a). In the coronal ST sections, both types of axon bundles, which were cut into rings or sectioned along with the fibers, were detected. In the ST, bundles of the Nav1.2-positive fibers and only a few NFH-positive fibers were observed (Fig. 11b). To detect the nodes of Ranvier, the sections were stained with the anti-Nav1.6 and anti-Caspr antibodies. The nodes of Ranvier were not identified on the Nav1.2-positive axons (Fig. 11c). On the contrary, they were observed on the NFH-positive axons (Fig. 11d). These results suggest that the Nav1.2-expressing ST axons might be unmyelinated. To further confirm this, I performed EM and immuno-EM analyses. The EM showed that the fascicles of axons in the ST were composed of many unmyelinated axons (Fig. 12a). The anti-Nav1.2 antibody stained the surface and the interior part of the unmyelinated axons but not the myelinated axons (Fig. 12b, left). On the contrary, the internal part covered by the myelin sheaths was labeled with the anti-NFH antibody (Fig. 12b, right). Taken together, I demonstrated that Nav1.2-positive unmyelinated axons exist in the ST.

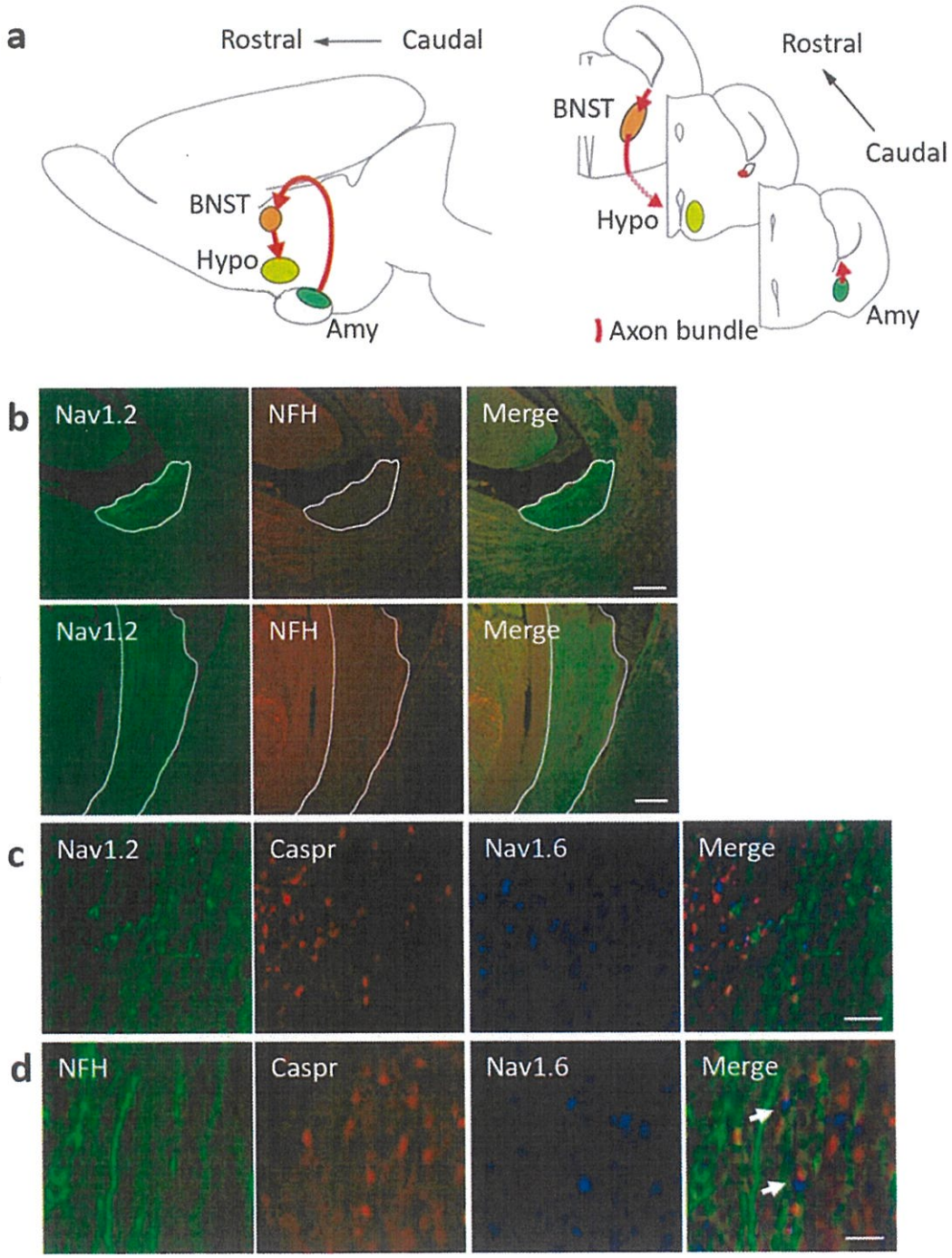
a
Rostral
Caudal
BNST
Hypo
Amy
Rostral
Caudal
BNST
Hypo
Amy
Axon bundle
b
Nav1.2
NFH
Merge
Nav1.2
NFH
Merge
c
Nav1.2
Caspr
Nav1.6
Merge
d
NFH
Caspr
Nav1.6
Merge

Figure 11. Characterization of the Nav1.2-expressing axons in the stria terminalis.

(a) a schematic diagram of the ST pathway. (b) The areas circled in white and the regions between the two white lines refer to the ST. (b-d) The coronal ST sections of the 8-week-old mice were stained with the following sets of antibodies: (b) anti-Nav1.2 (green) and anti-NFH (red), (c) anti-Nav1.2 (green), anti-Caspr (red) and anti-Nav1.6 (blue), and (d) anti-NFH (green), anti-Caspr (red) and anti-Nav1.6 (blue) antibodies. Arrows indicate the NFH-, Caspr- and Nav1.6-labeled axons. Scale bars: 100 μm (b, c), 20 μm (d).

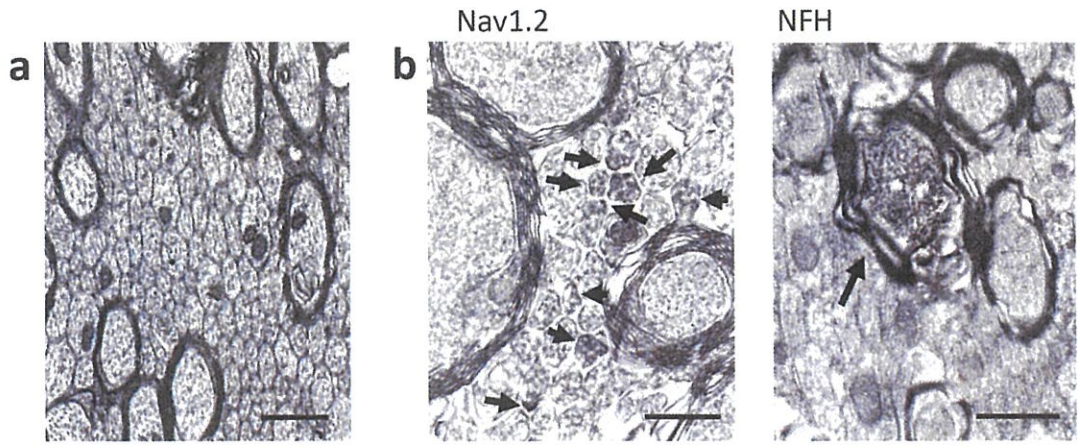

Figure 12. Unmyelinated axons in the stria terminalis.

(a) The EM analysis in the ST of the 8-week-old mice. (b) The immuno-EM analysis using the anti-Nav1.2 (left) and anti-NFH (right) antibodies in the ST fibers. Arrows indicate the Nav1.2- (left) and NFH- (right) labeled axons. Scale bars: 20 μm (a), 0.5 μm (b, left), 1.0 μm (b, right).

3. Discussion

In Chapter I, I examined the localization of unmyelinated fibers using the anti-Nav1.2 antibody in mouse brains with a hypothesis that Nav1.2 could be a marker of unmyelinated fibers.

A previous report of the localization of Nav1.2 on AIS and axon terminals of myelinated fibers (Ogiwara et al., 2018) raised questions about the specificity of the localization of Nav1.2 on the unmyelinated fibers. I demonstrated in CC and ST, the diffuse distribution of Nav1.2 on adult mouse mid-axons, which form axon bundles excluding AIS and axon terminals. Nav1.2 is diffusely localized on the axons in early stage of development and is progressively replaced by Nav1.6 during myelination (Boiko et al., 2001). I suppose in the Nav1.2-positive unmyelinated axons of early stage, the clustering of Nav1.6 occurs at the nodes of Ranvier only in the myelinated mid-axons (Fig. 13). Recently, the connectome study revealed partial myelination along axons of pyramidal neurons (Tomassy et al., 2014). We do not know whether in those axons Nav 1.2 is localized diffusely or other Navs exist. The relationship between those axons and the identified unmyelinated axons in this study should be further investigated.

I focused on the CC and ST in particular, the part of which were stained diffusely by the anti-Nav1.2 antibody. Then, I investigated the distribution of Nav1.2 on the unmyelinated fibers in the CC and ST by IHC and immuno-EM. Diffuse distribution of Nav1.2 in the CC and ST fibers, without the presence of the nodes of Ranvier, was observed. This suggests that the diffuse localization of Nav1.2 on the mid-axonal regions could be a useful marker of unmyelinated fibers in the CC and ST. However, Nav1.2-negative unmyelinated fibers were also observed by immuno-EM. Whether this is due to partial permeation of antibody through the membrane or unmyelinated axons expressing other types of Navs exist in the CC and ST should be studied further. The protemomic analysis of the axons of unmyelinated fibers may reveal whether Nav1.2 can be a universal marker for unmyelinated fibers or other Navs could be markers for specific types of unmyelinated axons.

While there have been many reports on myelinated axons, the roles of unmyelinated axons in the brain have not been well elucidated. To investigate the roles of unmyelinated axons in the brain network, I next searched for the origins of these unmyelinated axons in the CC and ST.

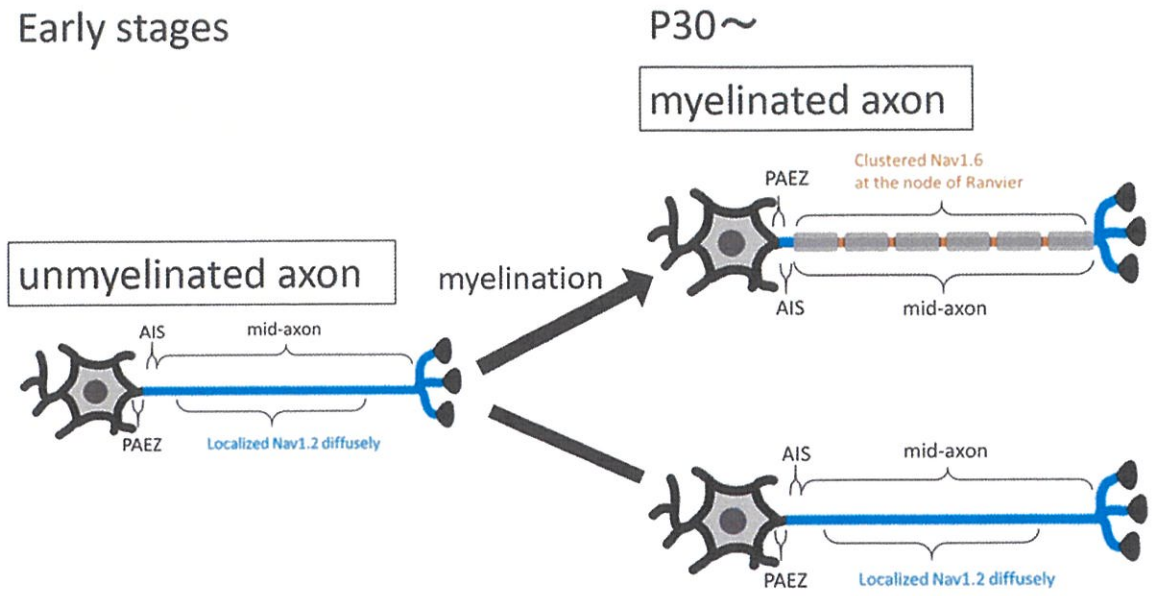

Figure 13. Changes in the structure of a mid-axon during the growth process.

Chapter Ⅱ. Searching for the cell bodies of neurons with unmyelinated axons in the corpus callosum and stria terminalis

1. Introduction

1.1. Estimating the location of the cell bodies of neurons with unmyelinated fibers.

In order to investigate the role of unmyelinated fibers in the brain network, the cell bodies of neurons with unmyelinated fibers should be identified first. I explored where the cell bodies of neurons with unmyelinated fibers of the CC and the ST come from. The part of the CC fibers is derived from the neurons in the cerebral cortex, and the ST fibers are projected from the amygdala (Ku and Torii, 2020, Dong et al., 2001). However, there are too many candidate regions for both the cerebral cortex and amygdala. To narrow it down, I hypothesized that the cell body diameter of unmyelinated fibers would be relatively small. There is a report that neuronal soma diameter correlates with axonal diameter in the callosal connections of the monkey (Fig. 14) (Tomasi et al., 2012). Also, the small neuronal cell bodies with a diameter of approximately 10 μm, granular cells, were found at the origin of the well-known unmyelinated fibers, such as hippocampal mossy fibers and cerebellar parallel fibers, in the CNS (Wyatt et al., 2005, Henze et al., 2000). Moreover, the neurons extending the striatal projection fibers, including medium spiny neurons, have a small diameter of approximately 12-13 μm (Miyazaki et al., 2014, Schmidt-Hieber et al., 2008, Wyatt et al., 2005, Bishop et al.,

1982). Since the part of the CC fibers are derived from the neurons in the cerebral cortex, and the ST fibers are projected from the amygdala (Ku and Torii, 2020, Dong et al., 2001), I assumed that unmyelinated axons in the CC and the ST are projected from the neurons with a diameter of approximately 10 μm in the cortex and amygdala, respectively.

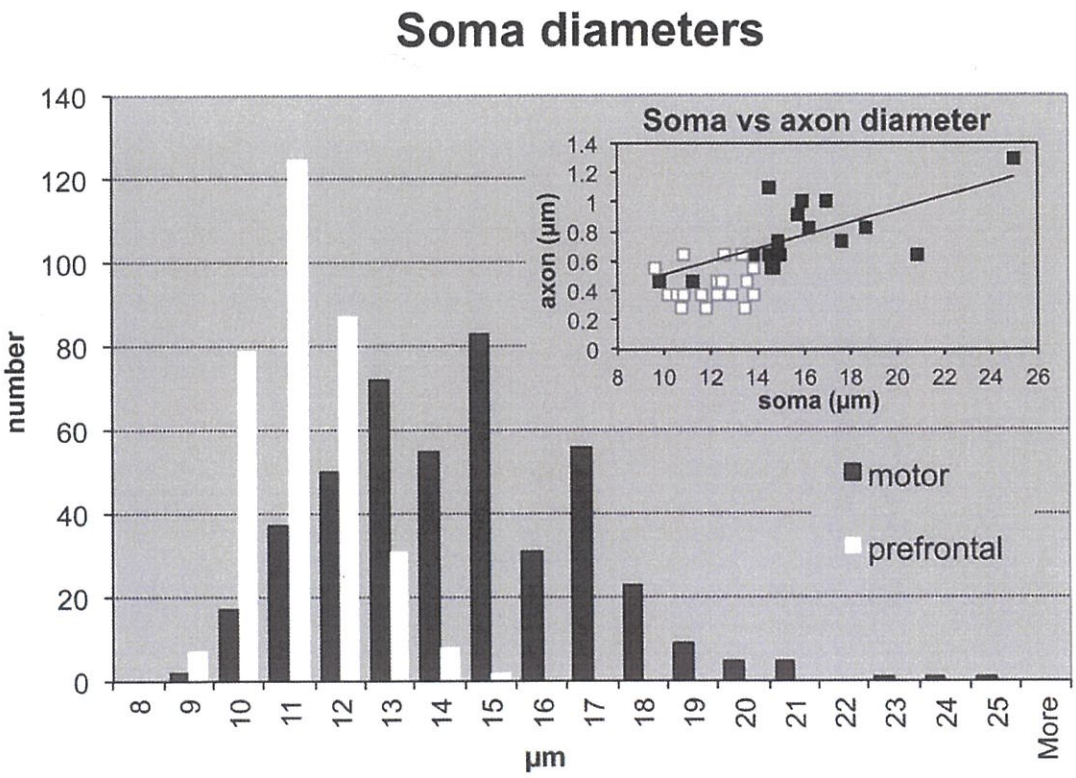

Figure 14. Distribution of soma diameters of the callosal projection neurons in the motor and prefrontal areas.

The callosal projection neurons were retrogradely labeled with biotinylated dextran amine (BDA). BDA, MW 3000 was injected in the corresponding contralateral sides in the

motor cortex and prefrontal cortex. The soma size and axon diameters of the labeled neurons were measured. Inset shows the relations between soma and axon diameters in individual callosal projection neurons in both areas, which are linearly correlated (Pearson = 0.73; $P<0.001$). The image was modified from (Tomasi et al., 2012).

1.2 Callosal projections.

The CC is the largest white matter tract that connects two cerebral hemispheres of placental animals. The communication via approximately two hundred million callosal axons allows efficient information exchange between the two hemispheres, coordinating our higher-order motor, sensory, and cognitive tasks (Paul et al., 2007, Paul, 2011). The human CC is anatomically divided into several regions that topographically connect two hemispheres: the anterior-most rostrum, genu, body, isthmus and splenium at the posterior end, while the mouse CC is usually divided into three regions: genu, body and splenium (Fig. 15 a, b). Along the anterior-posterior axis, the genu and rostrum connect the frontal and premotor regions of the cerebral cortex, the body conjoins the motor, somatosensory and parietal regions, while the splenium links the temporal and occipital cortices on both sides (Park et al., 2008, Putnam et al., 2010, Wahl et al., 2007). For

example, neuronal signals for the motor function pass through the genu, while somatosensory inputs go through the posterior body of the CC. Axons in isthmus are in charge of transmitting auditory signals, and visual information via splenium (Funnell et al., 2000, Blaauw and Meiners, 2020). Dorsal and ventral parts of the CC then connect the medial and lateral cortical regions, respectively (Fig. 15c).

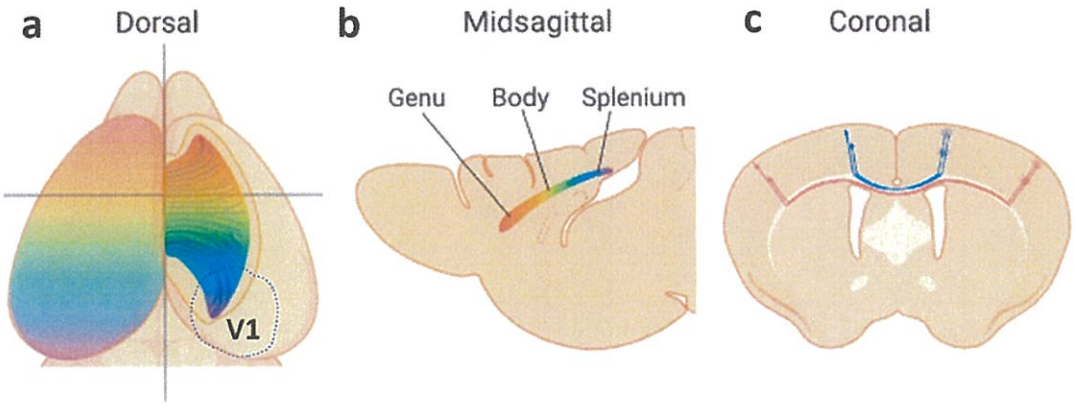

Figure 15. The organization of the mouse corpus callosum.

Dorsal (a), midsagittal (b), and coronal (c) views of the CC. Callosal axon projections from each cortical hemisphere cross the midline and primarily connect with homotopic cortical regions in a topographic manner, by which projections from anterior and posterior cortical regions form anterior and posterior parts of the CC, respectively (represented by rainbow colors in a and b). Callosal projections from the medial and lateral regions of the

cortex form the dorsal and ventral portions of the CC, respectively (c). The front part of the CC towards the frontal lobes is called the genu. The end part of the CC towards the cerebellum is called the splenium. V1, the primary visual cortex. The image was modified from (Ku and Torii, 2020).

1.3 Stria terminalis projections.

BST is a heterogeneous limbic forebrain structure comprising 12 subnuclei with distinct cytoarchitectural features and anatomical connectivity. In general, connections between the amygdala and the BST are topographically organized such that the anterolateral group of BST subnuclei is reciprocally connected with the central nucleus of the amygdala (CEA), comprising the "central extended amygdala" (Bienkowski and Rinaman, 2013, de Olmos and Heimer, 1999), whereas the anteromedial and posterior groups of BST subnuclei are reciprocally connected with the medial nucleus of the amygdala (Fig. 16), comprising the "medial extended amygdala" (de Olmos and Heimer, 1999).

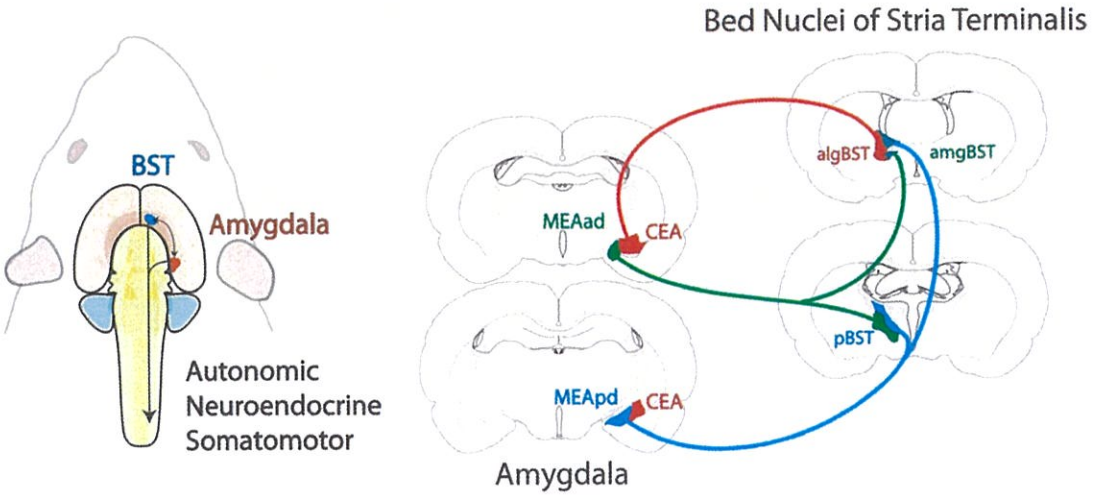

Figure 16. The amygdala and bed nucleus of the stria terminalis are densely interconnected.

The amygdala and BST coordinate autonomic, neuroendocrine, and somatomotor responses to internal and external stimuli and events (left). Results from anterograde tracing studies support the existence of topographically organized reciprocal connections between the amygdala and BST subnuclei (right). The CEA (red) is reciprocally connected to the anterolateral group of BST subnuclei (algBST), whereas the MEAad (green) and MEApd (blue) are reciprocally connected to complementary subregions of the posterior BST (pBST) and the anteromedial BST subnuclei group (amgBST). MEAad, medial nucleus of the amygdala, anterodorsal subnucleus; MEApd, medial nucleus of the amygdala, posterodorsal subnucleus. The image was modified from (Bienkowski et al., 2013).

1.4. The aim of this chapter.

While there have been many reports on myelinated fibers, the roles of unmyelinated fibers in the brain have not been well elucidated.

Figuring out whether the unmyelinated fibers are responsible for projection will help us understand the roles of the unmyelinated fibers. The part of the CC fibers is derived from the neurons in the cerebral cortex, and the ST fibers are projected from the amygdala. However, the exact area, where the unmyelinated fibers are projected from, has not been studied. To investigate the roles of unmyelinated fibers in the brain network, I next searched for the cell bodies of neurons with unmyelinated fibers in the CC and ST.

2. Results

2.1. The Nav1.2-positive fibers in the corpus callosum contain projection fibers from the primary visual cortex.

To estimate the location of the cell bodies of neurons with unmyelinated fibers, the anti-Nav1.2 antibody does not stain the cell body, I followed the Nav1.2-positive fibers before the cell body in the CC. The mouse brain sagittal sections were cut at 500 μm sequentially from the center to the lateral side. The bundles of the Nav1.2-positive fibers were separated up and down as they headed toward the lateral side of the brain (Fig. 17a). In the upper bundles, the Nav1.2-positive fibers were observed in the primary visual cortex (V1), which is the first cortical region that receives visual input (Fig. 17b) (Felleman and Van Essen, 1991). Therefore, the cell bodies of neurons with unmyelinated fibers could be detected as if they are located in the V1. The location of the cell bodies of neurons with unmyelinated fibers of the bottom bundles could not be examined.

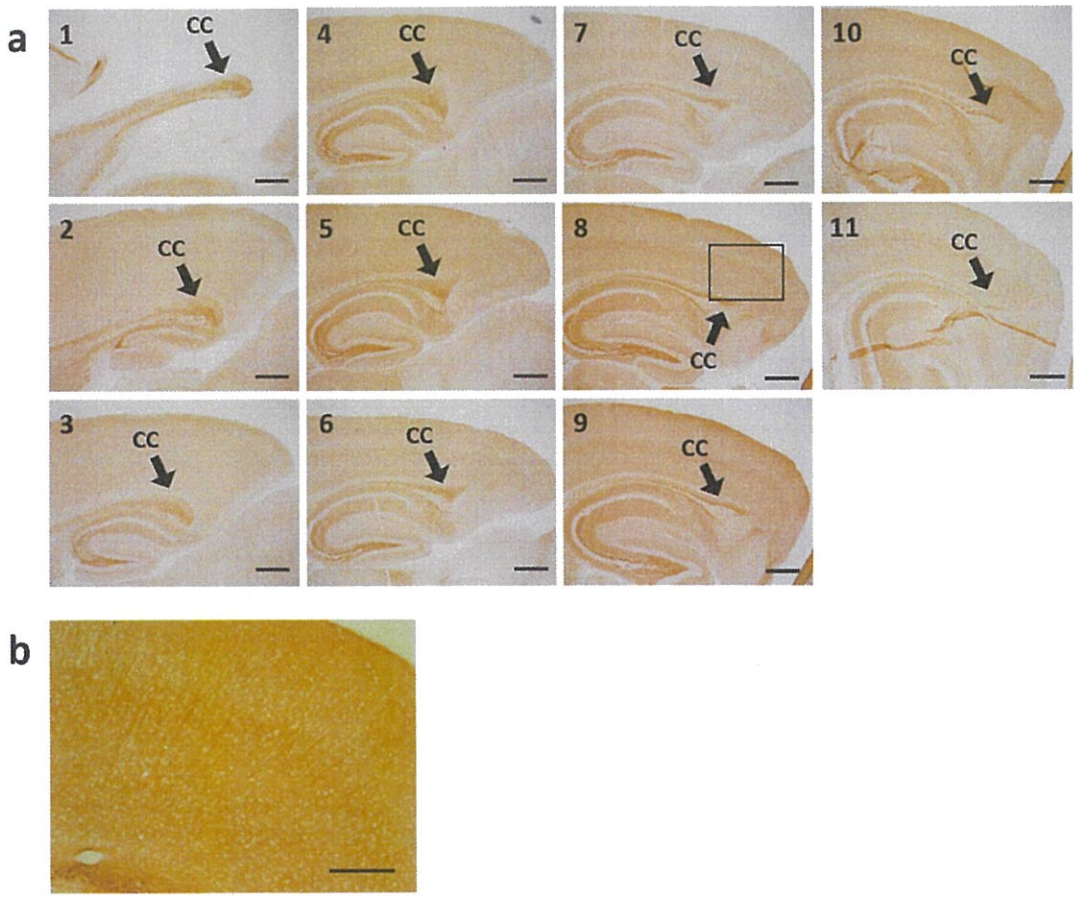

Figure 17. The Nav1.2-positive axons in the corpus callosum.

(a) The sagittal CC sections of the 8-week-old C57BL/6J mice were cut at 500 μm sequentially from the center (image 1) to the lateral side (image 11), and each section was stained with the anti-Nav1.2 antibody. The estimated location of the cell bodies of neurons with unmyelinated fibers was shown in the boxed area. (b) The image shows a higher magnification of the boxed area of image 8 in (a), which indicates the V1. Scale bars: 500 μm (a), 200 μm (b).

Then, I observed the projection of the neurons from the V1 after injecting BDA, an anterograde tracer, into the V1. BDA from the neuronal cell bodies with the size of 10 μm at the injection site traveled down the axons toward the terminal processes (Fig. 18a). However, it remained unclear which layer the BDA-injected cell bodies are located. In the V1, BDA in the cell bodies projected toward the contralateral side through the upper side of the CC (Fig. 18b). The location of the injection was in 3.5 mm caudal to the bregma, but the BDA-positive projection fibers were observed in the center of the CC bundles in 1.79 mm caudal to the bregma as well as in the contralateral side (Fig. 18c). Since the BDA-labeled fibers co-localized with the Nav1.2-positive fibers, I suggest that a part of the Nav1.2-positive fibers come from the V1 and project toward the contralateral side of the brain.

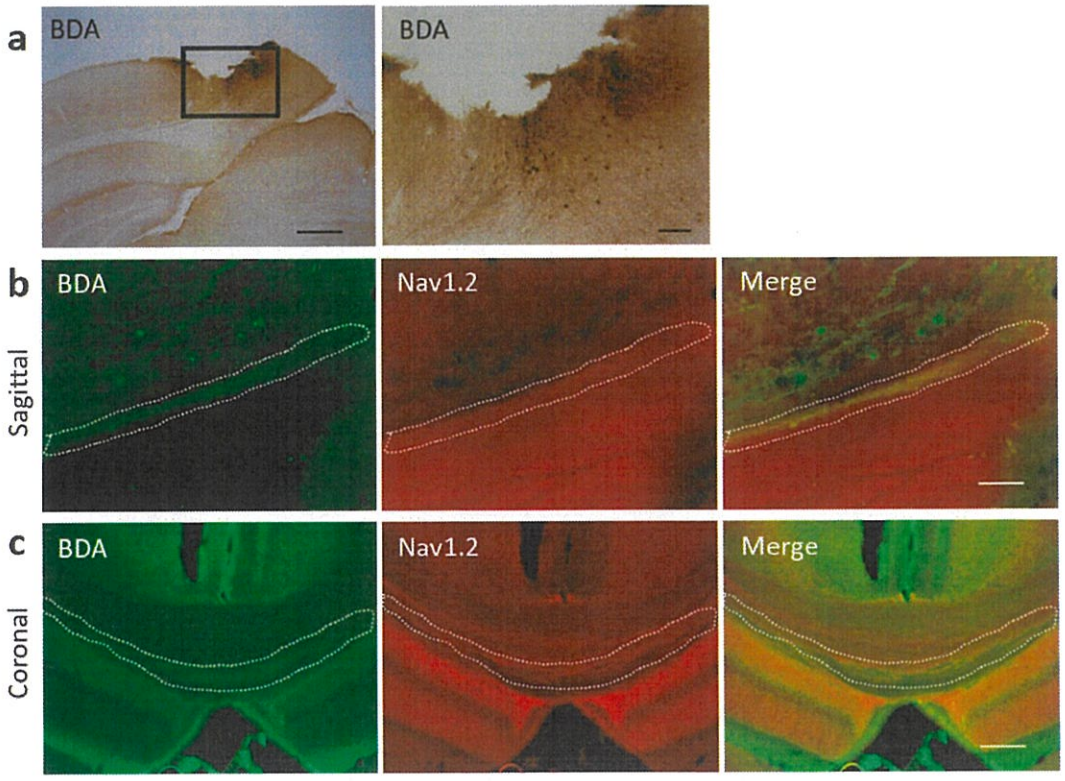

Figure 18. Projection from the primary visual cortex in the corpus callosum.

(a-c) BDA was injected into the V1 of the 8-week-old C57BL/6J mice. The injection site at (a, b) 3.5 mm caudal to the bregma and (c) 1.79 mm caudal to the bregma. (a) The immunostaining images of BDA. The right panel shows a higher magnification of the boxed area in the left panel. (b, c) The fluorescence images of the BDA (green) and the anti-Nav1.2 (red) antibody are shown. The areas circled in white dot lines refer to the BDA containing and the Nav1.2-labeled axons. Scale bars: 500 μm (a, left), 100 μm (a, right), 50 μm (b), 200 μm (c).

2.2. The tdTomato-positive neurons in the Scnn1a^{Cre}-tdTomato mice project unmyelinated and thin myelinated axons.

Next, I examined which cell layers the projection fibers came from. Because the fourth layer of the V1 (V1L4) is a thick granular cell layer, I hypothesized that the unmyelinated axons in the CC were projected from the V1L4. I prepared a mouse expressing *Scnn1a*^{Cre}-tdTomato which labeled the granular cells at the cortical L4 (Fig. 19a) (Harris et al., 2014). The *SCNN1A* gene encodes the α-subunit of the epithelial sodium channel, which is constitutively active and is not voltage-dependent. The function of *SCNN1A* in the brain has not been well elucidated. I observed the excitatory neurons labeled with tdTomato in the V1L4. The cells labeled with tdTomato had a small soma diameter of about 10 μm (Fig. 19b). Using this mouse, I examined whether these fibers from the cortical L4 were unmyelinated and found that most of the fibers projected through the bottom side of the fiber bundles in the CC (Fig. 19c, d). The Nav1.2-positive fibers and the projection fibers from the cortical L4 co-localized in a part of the fiber bundles in the center of the CC, suggesting that these fibers might be unmyelinated. However, other fiber bundles co-localized with NFH (Fig. 19e, f). Taken together, these

results suggest that both myelinated and unmyelinated fibers exist in the tdTomato-positive fibers.

Immuno-EM was performed to directly examine whether the tdTomato-positive fibers, which should come from the *Scnn1a*-expressing neurons, were unmyelinated. As a result, the tdTomato-positive fibers were detected in both myelinated and unmyelinated axons (Fig. 20a). The fibers from the V1L4 were not limited to the unmyelinated axons. Also, I focused on the thickness of axons to investigate which kind of neurons were tdTomato-positive. In the CC, some thick myelinated axons had a diameter of more than 1 μm, while some relatively thin myelinated axons had a diameter of 0.5 μm (Fig. 20b). The diameters of the tdTomato-positive axons were less than 0.5 μm regardless of whether they are myelinated or unmyelinated (Fig. 20c). Taken together, I suggest that the tdTomato-positive excitatory neurons project either thin myelinated or unmyelinated axons.

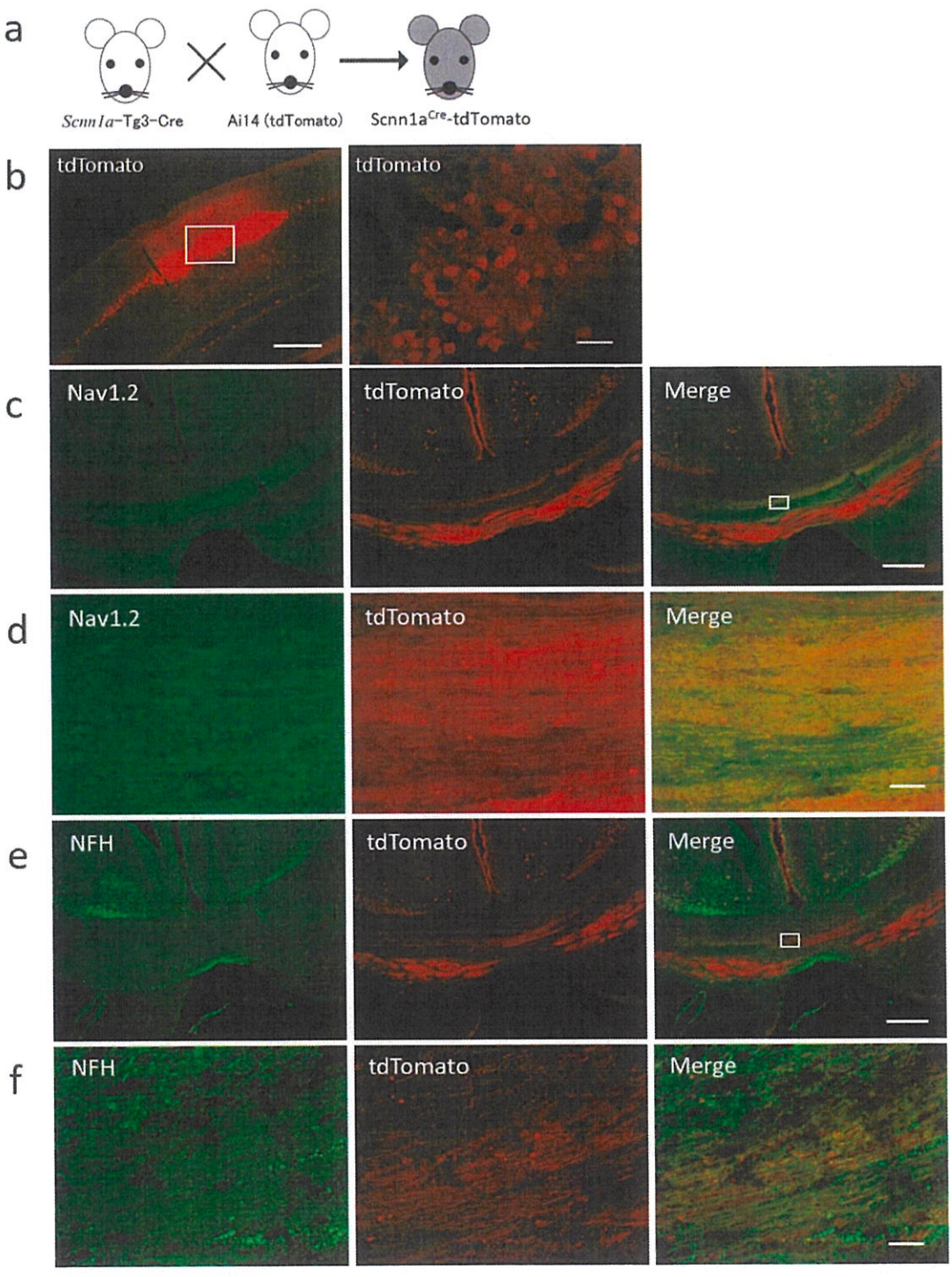
a
Scnn1a-Tg3-Cre
Ai14 (tdTomato)
Scnn1a^{Cre}-tdTomato
b
tdTomato
tdTomato
c
Nav1.2
tdTomato
Merge
d
Nav1.2
tdTomato
Merge
e
NFH
tdTomato
Merge
f
NFH
tdTomato
Merge

Figure 19. Projection fibers of the tdTomato-positive neurons in the corpus callosum.

(a) A schematic representation of a *Scnn1a*^{Cre}-tdTomato mouse. (b-f) The coronal sections of the 8-week-old *Scnn1a*^{Cre}-tdTomato mice were observed. (b) The tdTomato-positive neurons in the V1L4. The right panel shows a higher magnification of the boxed area in the left panel. (c-f) The brain sections of the *Scnn1a*^{Cre}-tdTomato mice were stained with the (c, d) anti-Nav1.2 (green) and anti-tdTomato (red) antibodies, and (e, f) anti-NFH (green) and anti-tdTomato (red) antibodies. (d) The panels show a higher magnification of the boxed area in the merged image in (c). (f) The panels show a higher magnification of the boxed area in the merged image in (e). Scale bars: 300 μm (b, left), 30 μm (b, right, d, f), 200 μm (c, e).

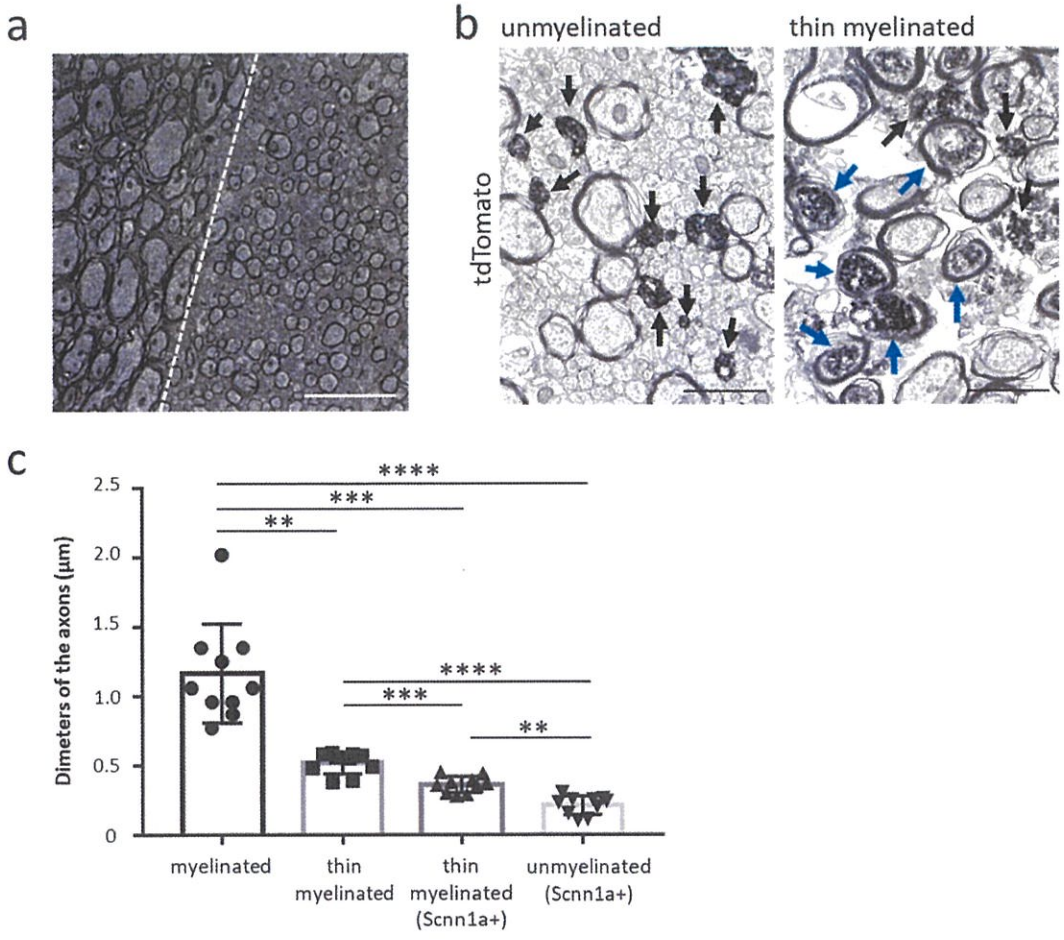

Figure 20. The diameters of axons in the corpus callosum of the *Scnn1a*^{Cre}-tdTomato mice.

(a) The EM analysis in the sagittal CC brain sections of the 8-week-old C57BL/6J mice was performed. The left side from the dotted line shows myelinated axons, and the right side from the dotted line shows thin myelinated axons. (b) The immuno-EM analysis in the sagittal CC brain sections of the 8-week-old *Scnn1a*^{Cre}-tdTomato mice was performed using the anti-RFP (red fluorescent protein) antibody. Arrows indicate the tdTomato-

positive unmyelinated axons (black) and the thin myelinated axons (blue). (c) The diameters of the myelinated, thin myelinated and unmyelinated axons. **P<0.01, ***P<0.001, ****P<0.0001. Scale bars: 5 μm (a), 0.5 μm (b).

2.3. The Nav1.2-positive fibers in the stria terminalis contain projection fibers from the central amygdala.

I next investigated the cell bodies of neurons with unmyelinated fibers, following the path of the Nav1.2-positive fibers in the ST. The sagittal brain sections were cut at 500 μm sequentially from the center to the lateral side of the brain. The Nav1.2-positive fibers were projected from the CEA, went through the medial in an arc shape (the boxed area of panel 9 in Fig. 21a, Fig 21b) and finally headed toward the BST. As previously reported, the CEA projects the BST (Fig. 16) (Bienkowski et al., 2013). Therefore, I assumed that the cell bodies of neurons with unmyelinated fibers came from the CEA.

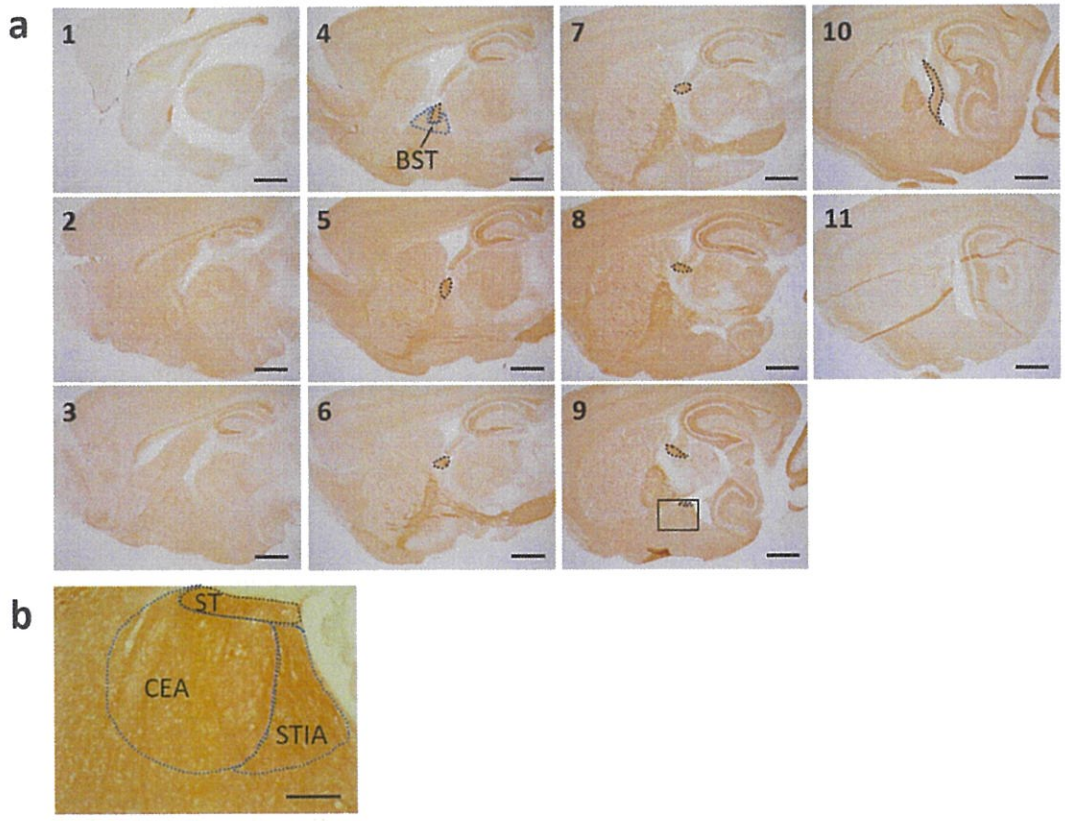

Figure 21. The Nav1.2-positive axons in the stria terminalis.

(a) The sagittal ST sections of the 8-week-old C57BL/6J mice were cut at 500 μm sequentially from the center (image 1) to the lateral side (image 11), and each section was stained with the anti-Nav1.2 antibody. The estimated location of the cell bodies of neurons with unmyelinated fibers was shown in the boxed area. The areas circled in black refer to the ST, and the regions circled in blue dot lines refer to the nucleus area. (b) The image shows a higher magnification of the boxed area of image 9 in (a). ST, stria

terminalis; BST, bed nucleus of the stria terminalis; CEA, central amygdala; STIA, bed nucleus of the stria terminalis, intraamygdaloid division. Scale bars: 1 mm (a), 200 μm (b).

3. Discussion

In Chapter II, I estimated the location of the cell bodies of neurons with unmyelinated fibers, following the path of the Nav1.2-positive fibers in the CC and ST, with a hypothesis that unmyelinated axons in the CC and the ST are projected from the neurons with a diameter of approximately 10 μm in the cortex and amygdala.

To identify the projection pathways, I first injected BDA, the anterograde tracer, into the V1 of the CC and observed the specifically fluorescence-labeled axons and somas of the V1. Since the BDA-labeled fibers co-localized with the Nav1.2-positive fibers, a part of the Nav1.2-positive fibers might come from the V1 and project toward the contralateral side of the brain. Next, to examine which cell layers the projection fibers came from, I prepared a mouse expressing *Scnn1a*^{Cre}-tdTomato which labels the granular cells at the cortical L4. However, the immuno-EM analysis suggested that the tdTomato-positive excitatory neurons project either thin myelinated or unmyelinated axons. In the ST, the cell bodies of neurons with unmyelinated fibers might come from the CEA, following the path of the Nav1.2-positive fibers. Taken together, the cell bodies of neurons with unmyelinated fibers in the CC and ST include small neurons in the cortex and amygdala. Allen Mouse Brain Connectivity Atlas showed that the V1 of the

Scnn1a^{Cre}-tdTomato mice project axons through CC, which could be unmyelinated. To identify the original neurons of these unmyelinated fibers, further studies using a virus and *Scnn1a*^{Cre} mice specifically expressing a marker in the limited cell types are necessary.

There are a lot of Nav1.2-positive and tdTomato-negative axons in the CC in the *Scnn1a*-Tg3-Cre mouse. It is estimated that 80% of callosal axons come from neurons in layer II/III, and 20% are from neurons in layer V in the mature brain (Fame et al., 2011). These layers of the cerebral cortex should also be observed.

Nav1.2 is expressed in many regions of the mammalian brain including the hippocampus, cerebellum and striatum (Gong et al., 1999, Yamagata et al., 2017). The clustering of sodium channels to generate action potentials at AIS evolved before the divergence of jawed and jawless vertebrates approximately 560 million years ago (Fig. 22) (Hill et al., 2008). Most fast-transmitting axons in jawed vertebrates (gnathostomata) are myelinated. On the contrary, jawless vertebrates (agnatha/ cyclostomata) including lamprey do not possess myelin and thus represent an ancestral stage in the vertebrate nervous system evolution (Bullock et al., 1984). Even though axonal myelination in the CNS began more than 500 million years ago, there must be an advantage to unmyelinated fibers to remain until today. However, the role of unmyelinated fibers in the CNS is still not well understood. In the CC, the vesicular release of glutamate from the unmyelinated

fibers was discovered (Fig. 23) (Kukley et al., 2007). The newly discovered unmyelinated fibers are all axon bundles. The bundling of many axons together and the exchange of vesicles between axons must have some inherent benefit in information transmission.

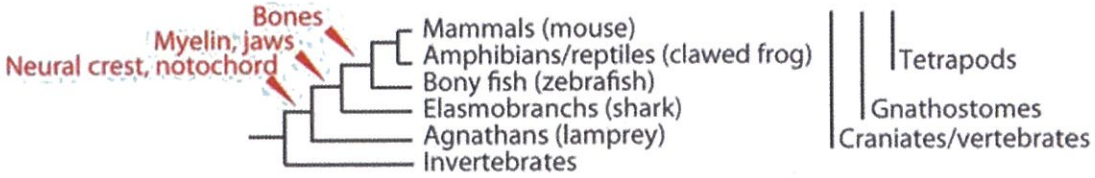

Figure 22. Evolutionary relationships of representative model species.

Consequential evolutionary innovations are indicated (red arrowheads). The image was modified from (Weil et al., 2018).

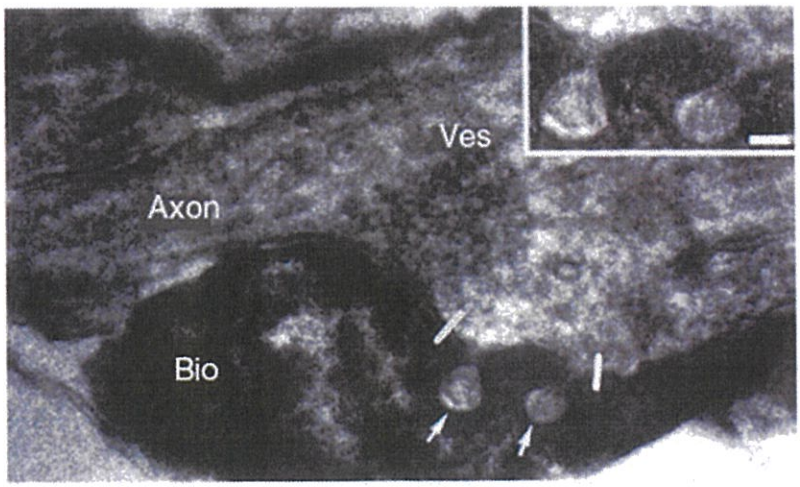

Figure 23. Unmyelinated axons contain synapse-like vesicles at contact sites with oligodendrocyte precursor cells.

The EM analysis of the relationship of biocytin-filled processes (Bio) of oligodendrocyte precursor cells with neighboring axons. The axon forms a small varicosity containing many vesicles (Ves). Note that small protrusions of the axonal membrane form glial invaginations (arrows). This shows a magnified view of invaginations between the white bars (inset scale bar: 50 nm). The image was modified from (Kukley et al., 2007).

Mutations of the *SCN2A* gene are associated with neurological disorders such as epilepsy, autism spectrum disorders, intellectual disabilities and schizophrenia (Hoischen et al., 2014). Nav1.2 is well expressed in excitatory neurons such as neocortical and hippocampal pyramidal cells, and therefore it can be naturally assumed that gain-of-function mutations of *SCN2A* lead to hyper-excitabilities of those excitatory neurons and result in epileptic seizures. Nav1.2 is densely expressed in unmyelinated axons of neurons in hippocampal dentate and cerebellar granule cells, while in striatum Nav1.2 is present at unmyelinated axons of GABAergic medium spiny neurons. Nav1.2 is also expressed

in neocortical somatostatin-positive inhibitory neurons but not in the parvalbumin-positive neurons (Ogiwara et al., 2018, Yamagata et al., 2017).

The CEA is a striatum-like output of the amygdala, consisting almost exclusively of GABAergic medium spiny neurons. Therefore, Nav1.2-positive axons might be GABAergic medium spiny neurons (Liu et al., 2021). The CEA has been proved to play a key role in the control of anxiety, stress and fear-related behaviors. The symptoms related to emotions of neurological disorders might be caused by mutations of the *SCN2A* gene in the CEA. The pathological role of Nav1.2 mutations or loss in unmyelinated fibers should be further investigated. I hope that investigating the localization and function of unmyelinated fibers in the CNS could contribute to elucidating the pathogenesis of the diseases and further developing treatments for the diseases.

Materials and Methods

Animals: The mouse experiments were approved by the animal experiment committee at Doshisha University. Mice were maintained and bred in accordance with the guidelines of Doshisha University. 8-week-old C57BL/6J mice were obtained from CLEA Japan, Inc. Only male mice were used for this study.

***Scnn1a*^{Cre}-tdTomato mice:** Adult *Scnn1a*-Tg3-Cre (B6; C3-Tg (*Scnn1a*-cre)3Aibs/J, RRID: IMSR_JAX:009613) and Ai14-reporter mice (B6; Cg-Gt (ROSA)26Sor$^{tm14\ (CAG-tdTomato)\ Hze}$ /J, RRID: IMSR_JAX:007914) were purchased from Jackson Labs. Heterozygous *Scnn1a*-cre mice were bred with homozygous Ai14-reporter mice. *Scnn1a* x Ai14 positive offspring constitutively expressed tdTomato in all cre-positive cells (*Scnn1a*^{Cre}-tdTomato).

Generation of an anti-Nav1.2 antibody: Rat monoclonal anti-Nav1.2 (1B6-1C1) antibody was generated against KLH-conjugated oligopeptides corresponding to the C-terminal region of human Nav1.2 (amino acids 466–485). Hybridoma supernatants were screened by ELISA, and then selected subclones were further analyzed by Western blot

and IHC. Conditioned media of a selected clone (1B6-1C1) were harvested from the stable hybridoma cultures, and the antibody was purified using a HiTrap SP HP column (GE Healthcare) by Cell Engineering Corporation (Osaka, Japan). The precise characterization of this monoclonal antibody (1B6-1C1) will be published elsewhere (Miyazaki, et al. unpublished). The antibody recognized the ~260KDa sized band, and IHC confirmed that the staining of striatal projection fibers disappeared in the *SCN2A* conditional knockout mouse.

Antibodies: The following primary antibodies were used: anti-NFH (1:1,000 for IHC and IF, 1:10,000 for immuno-EM, AB5539, Chemicon), anti-Nav1.2 (1:1,000 for IHC and IF, 1:500 for immuno-EM), anti-Nav1.6 (1:700 for IHC and IF), anti-Caspr clone K65/35 (1:1,000 for IHC and IF, 75-001, NeuroMab), anti-RFP (1:3000 for immuno-EM #M155-3, MBL International Corporation) antibodies.

For IHC and immuno-EM, the following secondary antibodies were used: Biotinylated anti-rat IgG (1:300 for IHC, 1:500 for immuno-EM, BA-9400, Vector), Biotinylated anti-mouse IgM (1:300 for IHC, 1:500 for immuno-EM, BA-2020, Vector) and Biotinylated anti-chicken IgY (IgG) (1:500 for immuno-EM, 703-065-155, Jackson ImmunoResearch) antibodies.

For IF, the following secondary antibodies were used after diluted by 1:300: Alexa Fluor 488 anti-rat IgG (A-11006, Invitrogen), Alexa Fluor 488 anti-chicken IgG (A-11039, Invitrogen), Alexa Fluor 546 anti-chicken IgG (A-11040, Invitrogen), Alexa Fluor 546 anti-mouse IgG (A-11030, Invitrogen) and Alexa Fluor 647 anti-rabbit IgG (A-21246, Invitrogen) antibodies.

Immunohistochemistry: Mice (C57BL/6J, N = 5; *Scnn1a*^{Cre}-tdTomato, N = 3) were perfused with phosphate buffered saline (PBS) and subsequently with 4% paraformaldehyde (PFA) in PBS. To prepare paraffin sections, brains were postfixed, dehydrated and embedded in paraffin wax. 5-μm-thick sections were cut with an HM430 sliding microtome (PHC). Autoclaved paraffin sections were quenched with 3% H_2O_2 in methanol for 30 min before blocking with 5% skim milk in TBST. The sections were then incubated in the primary antibodies diluted in TBST overnight at 4˚C, followed by the secondary antibody incubation at room temperature for 30 min. The sections were then incubated with VECTASTAIN Elite ABC Kit (Vector Laboratories) for 30 min. The signals were developed with substrate solution containing 0.1% diaminobenzidine (DAB), 0.015% H_2O_2 and 0.05 M Tris-HCl (pH 7.6). Images were taken with BIOREVO BZ-

9000 (KEYENCE), and we captured approximately the same area in each comparative sample.

Immunofluorescence: Mice (C57BL/6J, N = 5; *Scnn1a*^{Cre}-tdTomato, N = 5) were perfused with PBS and subsequently with 4% PFA in PBS. To prepare frozen sections, brains were postfixed by 4% PFA in PBS overnight, immersed in 30% sucrose in PBS, embedded in OCT compound, immediately frozen by liquid N_2 and stored at -80°C. The brains were sectioned at 20 μm with a cryostat (CM1860, Leica). The sections were blocked with 5% skim milk in TBST for 1 h and incubated with the primary antibodies diluted in TBST overnight at 4°C, followed by the secondary antibody incubation at room temperature for 30 min. All images were taken with BIOREVO BZ-9000 (KEYENCE), and we captured approximately the same area in each comparative sample.

Analysis of axon distribution from the V1: 5% BDA (D1956, Invitrogen) in PBS was injected into the V1 (AP: 3.5 mm caudal to the bregma, LM: 2.16 mm lateral from the midline, depth: 0.5 mm from the pial surface) using a glass pipette (tip diameter, 15-20 μm). 3 days after the tracer injection, each mouse (C57BL/6J, N = 15) was perfused with PBS and subsequently with 4% PFA in PBS. To prepare frozen sections, brains were

postfixed by 4% PFA in PBS overnight, immersed in 30% sucrose in PBS, embedded in OCT compound and immediately frozen by liquid N_2 and stored at -80°C. The brains were sectioned at 50 μm with an electro freeze (MC-802C, yamatokoki) on the HM430 sliding microtome (PHC). The slices were incubated with 0.3% H_2O_2 in PBS (0.2% TritonX-100) for 30 minutes, followed by the incubation in blocking solution (2% BSA in TBST) for 1 h. The slices were then transferred to the primary antibody solution containing 2% BSA in TBST overnight at 4°C, incubated with the biotinylated secondary antibody solution containing 2% BSA in TBST for 3 h, and then incubated with streptavidin conjugated with CF488 (1:4000, #29034, Biotium) for 5 h at 4°C.

Transmission EM: For EM, mice (C57BL/6J, N = 4) were perfused with 2% PFA, 2.5% glutaraldehyde and 0.1 M sodium cacodylate (pH 7.4). The coronal sections of the ST and the sagittal sections of the CC (500-μm-thick) were cut with a vibratome, followed by the post-fixation with 2% OsO_4 in the same buffer. Fixed specimens were dehydrated with a graded series of ethanol and embedded in Epok812 (Oken shoji). Ultrathin sections were cut and stained with lead citrate. These sections were examined with an HT7700 transmission electron microscope (Hitachi).

Pre-embedding immuno-EM: For immune-EM, mice (C57BL/6J, N = 4; *Scnn1a*^{Cre}-tdTomato, N = 4) were perfused with 2% PFA, 1% glutaraldehyde and 0.1 M sodium cacodylate (pH 7.4). The coronal sections of the ST and the sagittal sections of the CC (200-μm-thick each) were cut with a vibratome. The slices were frozen and thawed with TBS three times and incubated with 0.1% H_2O_2 in TBS for 1.5 h, followed by the incubation in blocking solution (2% BSA in TBS) for 2 h. The slices were transferred to the primary antibody solution containing 2% BSA in TBS overnight at 4°C, incubated with the biotinylated secondary antibody solution containing 2% BSA in TBS for 3 h, and then incubated with ABC reagent of VECTASTAIN Elite ABC Kit (Vector Laboratories) for 2 h and subsequently developed with DAB substrate solution (5 mg DAB and 1.2 μl 30% H_2O_2 in 40 ml 0.05M Tris–HCl (pH 7.4)) for 20 min. Post-fixation was performed with 2% OsO_4 in the same buffer. The fixed specimens were dehydrated with a graded series of ethanol and embedded in Epok812 (Oken shoji). Ultrathin sections were cut and stained with lead citrate. These sections were examined with an HT7700 transmission electron microscope (Hitachi).

Data analysis: Multiple comparisons were conducted by one-way ANOVA followed by Tukey's posttest. P-values less than 0.05 were evaluated as statistically significant. Data were analyzed by GraphPad Prism 7.0 software (SanDiego, CA, USA).

References

AKOPIAN, A. N., SOUSLOVA, V., ENGLAND, S., OKUSE, K., OGATA, N., URE, J., SMITH, A., KERR, B. J., MCMAHON, S. B., BOYCE, S., HILL, R., STANFA, L. C., DICKENSON, A. H. & WOOD, J. N. 1999. The tetrodotoxin-resistant sodium channel SNS has a specialized function in pain pathways. *Nat Neurosci,* 2, 541-8.

BANT, J. S. & RAMAN, I. M. 2010. Control of transient, resurgent, and persistent current by open-channel block by Na channel beta4 in cultured cerebellar granule neurons. *Proc Natl Acad Sci U S A,* 107, 12357-62.

BARONI, D. & MORAN, O. 2015. On the multiple roles of the voltage gated sodium channel β 1 subunit in genetic diseases. *Front Pharmacol,* 6, 108.

BIENKOWSKI, M. S. & RINAMAN, L. 2013. Common and distinct neural inputs to the medial central nucleus of the amygdala and anterior ventrolateral bed nucleus of stria terminalis in rats. *Brain Struct Funct,* 218, 187-208.

BIENKOWSKI, M. S., WENDEL, E. S. & RINAMAN, L. 2013. Organization of multisynaptic circuits within and between the medial and the central extended amygdala. *J Comp Neurol,* 521, 3406-31.

BISHOP, G. A., CHANG, H. T. & KITAI, S. T. 1982. Morphological and physiological properties of neostriatal neurons: an intracellular horseradish peroxidase study in the rat. *Neuroscience,* 7, 179-91.

BLAAUW, J. & MEINERS, L. C. 2020. The splenium of the corpus callosum: embryology, anatomy, function and imaging with pathophysiological hypothesis. *Neuroradiology,* 62, 563-585.

BLACK, J. A., CUMMINS, T. R., PLUMPTON, C., CHEN, Y. H., HORMUZDIAR, W., CLARE, J. J. & WAXMAN, S. G. 1999. Upregulation of a silent sodium channel after peripheral, but not central, nerve injury in DRG neurons. *J Neurophysiol,* 82, 2776-85.

BOIKO, T., RASBAND, M. N., LEVINSON, S. R., CALDWELL, J. H., MANDEL, G., TRIMMER, J. S. & MATTHEWS, G. 2001. Compact myelin dictates the differential targeting of two sodium channel isoforms in the same axon. *Neuron,* 30, 91-104.

BULLOCK, T. H., MOORE, J. K. & FIELDS, R. D. 1984. Evolution of myelin sheaths: both lamprey and hagfish lack myelin. *Neurosci Lett,* 48, 145-8.

CASTELFRANCO, A. M. & HARTLINE, D. K. 2016. Evolution of rapid nerve conduction. *Brain Res,* 1641, 11-33.

CATTERALL, W. A. 2012. Voltage-gated sodium channels at 60: structure, function and pathophysiology. *J Physiol,* 590, 2577-89.

DE OLMOS, J. S. & HEIMER, L. 1999. The concepts of the ventral striatopallidal system and extended amygdala. *Ann N Y Acad Sci,* 877, 1-32.

DONG, H. W., PETROVICH, G. D. & SWANSON, L. W. 2001. Topography of projections from amygdala to bed nuclei of the stria terminalis. *Brain Res Brain Res Rev,* 38, 192-246.

FAME, R. M., MACDONALD, J. L. & MACKLIS, J. D. 2011. Development, specification, and diversity of callosal projection neurons. *Trends Neurosci,* 34, 41-50.

FELLEMAN, D. J. & VAN ESSEN, D. C. 1991. Distributed hierarchical processing in the primate cerebral cortex. *Cereb Cortex,* 1, 1-47.

FELTENSTEIN, M. W. & SEE, R. E. 2008. The neurocircuitry of addiction: an overview. *Br J Pharmacol,* 154, 261-74.

FUNNELL, M. G., CORBALLIS, P. M. & GAZZANIGA, M. S. 2000. Cortical and subcortical interhemispheric interactions following partial and complete callosotomy. *Arch Neurol,* 57, 185-9.

GOLDIN, A. L. 2001. Resurgence of sodium channel research. *Annu Rev Physiol,* 63, 871-94.

GONG, B., RHODES, K. J., BEKELE-ARCURI, Z. & TRIMMER, J. S. 1999. Type I and type II Na(+) channel alpha-subunit polypeptides exhibit distinct spatial and temporal patterning, and association with auxiliary subunits in rat brain. *J Comp Neurol,* 412, 342-52.

HARRIS, J. A., HIROKAWA, K. E., SORENSEN, S. A., GU, H., MILLS, M., NG, L. L., BOHN, P., MORTRUD, M., OUELLETTE, B., KIDNEY, J., SMITH, K. A., DANG, C., SUNKIN, S., BERNARD, A., OH, S. W., MADISEN, L. & ZENG, H. 2014. Anatomical characterization of Cre driver mice for neural circuit mapping and manipulation. *Front Neural Circuits,* 8, 76.

HENZE, D. A., URBAN, N. N. & BARRIONUEVO, G. 2000. The multifarious hippocampal mossy fiber pathway: a review. *Neuroscience,* 98, 407-27.

HILDEBRAND, C., BOWE, C. M. & REMAHL, I. N. 1994. Myelination and myelin sheath remodelling in normal and pathological PNS nerve fibres. *Prog Neurobiol,* 43, 85-141.

HILDEBRAND, C., REMAHL, S., PERSSON, H. & BJARTMAR, C. 1993. Myelinated nerve fibres in the CNS. *Prog Neurobiol,* 40, 319-84.

HILL, A. S., NISHINO, A., NAKAJO, K., ZHANG, G., FINEMAN, J. R., SELZER, M. E., OKAMURA, Y. & COOPER, E. C. 2008. Ion channel clustering at the axon initial segment and node of Ranvier evolved sequentially in early chordates. *PLoS Genet,* 4, e1000317.

HOISCHEN, A., KRUMM, N. & EICHLER, E. E. 2014. Prioritization of neurodevelopmental disease genes by discovery of new mutations. *Nat Neurosci,* 17, 764-72.

KU, R. Y. & TORII, M. 2020. New Molecular Players in the Development of Callosal Projections. *Cells,* 10.

KUKLEY, M., CAPETILLO-ZARATE, E. & DIETRICH, D. 2007. Vesicular glutamate release from axons in white matter. *Nat Neurosci,* 10, 311-20.

LAI, H. C. & JAN, L. Y. 2006. The distribution and targeting of neuronal voltage-gated ion channels. *Nat Rev Neurosci,* 7, 548-62.

LI, T., TIAN, C., SCALMANI, P., FRASSONI, C., MANTEGAZZA, M., WANG, Y., YANG, M., WU, S. & SHU, Y. 2014. Action potential initiation in neocortical inhibitory interneurons. *PLoS Biol,* 12, e1001944.

LIU, J., HU, T., ZHANG, M. Q., XU, C. Y., YUAN, M. Y. & LI, R. X. 2021. Differential efferent projections of GABAergic neurons in the basolateral and central nucleus of amygdala in mice. *Neurosci Lett,* 745, 135621.

MANGIARINI, L., SATHASIVAM, K., SELLER, M., COZENS, B., HARPER, A., HETHERINGTON, C., LAWTON, M., TROTTIER, Y., LEHRACH, H., DAVIES, S. W. & BATES, G. P. 1996. Exon 1 of the HD gene with an expanded CAG repeat is sufficient to cause a progressive neurological phenotype in transgenic mice. *Cell,* 87, 493-506.

MIYAZAKI, H., OYAMA, F., INOUE, R., AOSAKI, T., ABE, T., KIYONARI, H., KINO, Y., KUROSAWA, M., SHIMIZU, J., OGIWARA, I., YAMAKAWA, K., KOSHIMIZU, Y., FUJIYAMA, F., KANEKO, T., SHIMIZU, H., NAGATOMO, K., YAMADA, K., SHIMOGORI, T., HATTORI, N., MIURA, M. & NUKINA, N. 2014. Singular localization of sodium channel $\beta 4$ subunit in unmyelinated fibres and its role in the striatum. *Nat Commun,* 5, 5525.

NIRSCHL, J. J., GHIRETTI, A. E. & HOLZBAUR, E. L. F. 2017. The impact of cytoskeletal organization on the local regulation of neuronal transport. *Nat Rev Neurosci,* 18, 585-597.

OGIWARA, I., MIYAMOTO, H., TATSUKAWA, T., YAMAGATA, T., NAKAYAMA, T., ATAPOUR, N., MIURA, E., MAZAKI, E., ERNST, S. J., CAO, D., OHTANI, H., ITOHARA, S., YANAGAWA, Y., MONTAL, M., YUZAKI, M., INOUE, Y., HENSCH, T. K., NOEBELS, J. L. & YAMAKAWA, K. 2018. Nav1.2 haplodeficiency in excitatory neurons causes absence-like seizures in mice. *Commun Biol,* 1, 96.

OYAMA, F., MIYAZAKI, H., SAKAMOTO, N., BECQUET, C., MACHIDA, Y., KANEKO, K., UCHIKAWA, C., SUZUKI, T., KUROSAWA, M., IKEDA, T., TAMAOKA, A., SAKURAI, T. & NUKINA, N. 2006. Sodium channel beta4 subunit: down-regulation and possible involvement in neuritic degeneration in Huntington's disease transgenic mice. *J Neurochem,* 98, 518-29.

PARK, H. J., KIM, J. J., LEE, S. K., SEOK, J. H., CHUN, J., KIM, D. I. & LEE, J. D. 2008. Corpus callosal connection mapping using cortical gray matter parcellation and DT-MRI. *Hum Brain Mapp,* 29, 503-16.

PAUL, L. K. 2011. Developmental malformation of the corpus callosum: a review of typical callosal

development and examples of developmental disorders with callosal involvement. *J Neurodev Disord,* 3, 3-27.

PAUL, L. K., BROWN, W. S., ADOLPHS, R., TYSZKA, J. M., RICHARDS, L. J., MUKHERJEE, P. & SHERR, E. H. 2007. Agenesis of the corpus callosum: genetic, developmental and functional aspects of connectivity. *Nat Rev Neurosci,* 8, 287-99.

PUTNAM, M. C., STEVEN, M. S., DORON, K. W., RIGGALL, A. C. & GAZZANIGA, M. S. 2010. Cortical projection topography of the human splenium: hemispheric asymmetry and individual differences. *J Cogn Neurosci,* 22, 1662-9.

SALIANI, A., PERRAUD, B., DUVAL, T., STIKOV, N., ROSSIGNOL, S. & COHEN-ADAD, J. 2017. Axon and Myelin Morphology in Animal and Human Spinal Cord. *Front Neuroanat,* 11, 129.

SCHMIDT-HIEBER, C., JONAS, P. & BISCHOFBERGER, J. 2008. Action potential initiation and propagation in hippocampal mossy fibre axons. *J Physiol,* 586, 1849-57.

TOLEDO-ARAL, J. J., MOSS, B. L., HE, Z. J., KOSZOWSKI, A. G., WHISENAND, T., LEVINSON, S. R., WOLF, J. J., SILOS-SANTIAGO, I., HALEGOUA, S. & MANDEL, G. 1997. Identification of PN1, a predominant voltage-dependent sodium channel expressed principally in peripheral neurons. *Proc Natl Acad Sci U S A,* 94, 1527-32.

TOMASI, S., CAMINITI, R. & INNOCENTI, G. M. 2012. Areal differences in diameter and length of corticofugal projections. *Cereb Cortex,* 22, 1463-72.

TOMASSY, G. S., BERGER, D. R., CHEN, H. H., KASTHURI, N., HAYWORTH, K. J., VERCELLI, A., SEUNG, H. S., LICHTMAN, J. W. & ARLOTTA, P. 2014. Distinct profiles of myelin distribution along single axons of pyramidal neurons in the neocortex. *Science,* 344, 319-24.

WAHL, M., LAUTERBACH-SOON, B., HATTINGEN, E., JUNG, P., SINGER, O., VOLZ, S., KLEIN, J. C., STEINMETZ, H. & ZIEMANN, U. 2007. Human motor corpus callosum: topography, somatotopy, and link between microstructure and function. *J Neurosci,* 27, 12132-8.

WEIL, M. T., HEIBECK, S., TöPPERWIEN, M., TOM DIECK, S., RUHWEDEL, T., SALDITT, T., RODICIO, M. C., MORGAN, J. R., NAVE, K. A., MöBIUS, W. & WERNER, H. B. 2018. Axonal Ensheathment in the Nervous System of Lamprey: Implications for the Evolution of Myelinating Glia. *J Neurosci,* 38, 6586-6596.

WYATT, K. D., TANAPAT, P. & WANG, S. S. 2005. Speed limits in the cerebellum: constraints from myelinated and unmyelinated parallel fibers. *Eur J Neurosci,* 21, 2285-90.

YAMAGATA, T., OGIWARA, I., MAZAKI, E., YANAGAWA, Y. & YAMAKAWA, K. 2017. Nav1.2 is expressed in caudal ganglionic eminence-derived disinhibitory interneurons: Mutually exclusive distributions of Nav1.1 and Nav1.2. *Biochem Biophys Res Commun,*

491, 1070-1076.